Nanoscale Advances

ROYAL SOCIETY OF CHEMISTRY

REVIEW

View Article Online
View Journal | View Issue

Cite this: *Nanoscale Adv.*, 2022, **4**, 1926

Fluorescence sensing by carbon nanoparticles

Rossella Santonocito, [a] Manuelamaria Intravaia, [a] Ivana Maria Caruso, [a] Andrea Pappalardo, [ab] Giuseppe Trusso Sfrazzetto *[ab] and Nunzio Tuccitto [ac]

Received 30th January 2022
Accepted 20th March 2022

DOI: 10.1039/d2na00080f

rsc.li/nanoscale-advances

Sensing is one of the most important fields in which chemists, engineers and other scientists are involved to realize sensoristic devices that can detect different analytes, both chemicals and biologicals. In this context, fluorescence sensing paves the way for the realization of smart sensoristic devices due to the possibility to detect the target analyte *via* a change in colour or emission. Recently (since 2006), carbon nanoparticles, which are a "new class" of nanostructures based on carbon atoms, have been widely used in sensing applications due to their intriguing optical properties. The scientific literature on this topic started from 2006 and a progressive increase in the corresponding number of publications has been observed. This review summarises the application of carbon nanoparticles in the sensing field, focusing on chemical and ion sensing.

Introduction

Nanostructures based on carbon atoms include different classes of organic compounds, such as fullerenes, graphene, nanotubes, nanodiamonds, and most recently carbon nanoparticles (CNPs). All these chemical species contain mainly sp^2 carbon atoms, but differ in their spatial evolution. In fact, fullerenes and carbon nanoparticles can be classified as zero-dimensional nanostructures, carbon nanotubes are one-dimensional objects, and graphene sheets are two-dimensional species (Fig. 1a).[1,2] In particular, CNPs represent quasi-spherical nanostructures with a diameter of a few nanometers, in the range if 3–10 nm in most of the cases.[3] The core of these materials, represented by a few graphene sheets assembled together, consists of nanocrystalline graphitic sp^2 carbon atoms, with some sp^3 defects.[4] The number of these sheets, having a distance of 0.334 nm from each other, tunes the height of the nanoparticle. The external shell, which is more interesting from a chemical point of view, contains different functional groups, whose nature depends on the synthetic methodology and the starting materials used to prepare the

[a]*Department of Chemical Sciences, University of Catania, 95125 Catania, Italy. E-mail: giuseppe.trusso@unict.it*

[b]*National Interuniversity Consortium for Materials Science and Technology (I.N.S.T.M.), Research Unit of Catania, 95125 Catania, Italy*

[c]*Laboratory for Molecular Surfaces and Nanotechnology – CSGI, 95125 Catania, Italy*

Rossella Santonocito was born in Catania, in 1996. She achieved her Bachelor's Degree in Chemistry in July 2019, working on the synthesis of new metal catalysts for the conversion of CO_2 into organic cyclic carbonates, and a Master's Degree in Chemical Sciences (Organic and Bioorganic Chemistry, University of Catania, Italy), in July 2021 with a score of 110/110 cum laude, working on the synthesis and application of new nanosensors for the supramolecular detection of explosives. She is currently a PhD student in Chemical Sciences at the University of Catania, working on the realization of multi-array sensors to detect biomarkers of human stress.

Manuelamaria Intravaia received her Bachelor's Degree in Chemistry in 2021 from the University of Catania (Italy), working on the synthesis of fluorescent sensors for the detection of nerve agents. Currently, she is a Master's student in the chemical sciences, organic and bioorganic chemistry curriculum at the University of Catania.

nanoparticles. Considering these factors, the starting organic material defines the composition of the external shell in terms of functional groups. For example, starting from a carboxylic acid, CNPs will show carboxylic groups on their external shell.[5] In the case of aromatic amines as the starting reagent, the final CNPs will be decorated by amino groups (Fig. 1b).[6] Due to the presence of many ionizable functional groups on their surface, native CNPs show good stability in water, thus leading to many biological applications and very low cytotoxicity.[7]

Furthermore, by exploiting the presence of these functional groups and their reactivity, CNPs can be covalently functionalized, anchoring a specific molecule having precise functionality on their surface.

CNPs are also characterized by chemical stability and notable photobleaching properties,[8,9] which allow their use in fluorescence bioimaging and biosensing. Their chemical stability is demonstrated by their resistance to a wide pH range (3–12) and strong fluorescence signal for months. The target of this review is to summarize the applications of carbon nanoparticles in the sensing field, focusing on chemical and ion sensing. In particular, chemical sensing will be classified by the function of the analyte. Similarly, ion sensing will be divided according to the function of the different metal ions detected. Also, because some recent reviews presented the biological applications of CNPs, such as intracellular imaging and theranostic use, these topics are not included in this review.[10–15]

Synthesis and optical properties of carbon nanoparticles

CNPs were first obtained by Xu *et al.* during the purification of single-walled carbon nanotubes through preparative electrophoresis in 2004,[16] and 2006 by Sun *et al. via* laser ablation of a carbon target.[17]

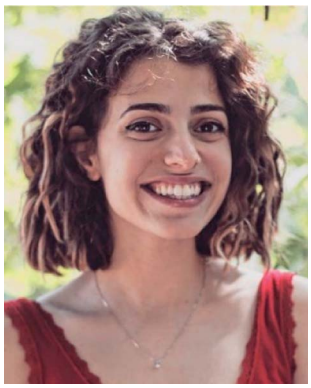

Ivana Maria Caruso was born in Catania in 1997. She received her Bachelor's Degree in Chemistry in July 2021, working on the design of a new fluorescent sensor for the supramolecular sensing of nerve agents, in the Laboratory of Supramolecular Organic Synthesis (LabSOrS) of Professor Giuseppe Trusso Sfrazzetto. She is currently a Master's student in Chemical Sciences of the University of Catania.

Giuseppe Trusso Sfrazzetto achieved his Master's Degree in Organic and Bioorganic Chemistry in 2007 with 110/110 cum laude at the University of Catania (Italy), working on new macrocyclic cavitands for enantioselective molecular recognition. He achieved his PhD in Chemical Sciences in 2011, discussing his thesis entitled "Design and synthesis of novel macrocyclic cavitands". His research is focused on new methods for the selective and green oxidation of organic substrates and new fluorescent sensors to detect important analytes. Since 2021, he has been an Associate Professor of Organic Chemistry in the Department of Chemical Sciences, in the University of Catania (Italy).

Prof. Andrea Pappalardo was born in Catania, Italy in 1974. After receiving his BS Degree in Chemistry and Pharmaceutical Technologies from Catania University in 1999, he continued his PhD study in Catania under the supervision of Prof. Gaetano Tomaselli. In 2004, he held a postdoctoral position at the Department of Organic and Biological Chemistry of the University of Messina under the supervision of Prof. Melchiorre Parisi. Since 2015, he has been a Professor at the Department of Chemical Science of the University of Catania. His research interests are focused on calixarene macrocycles and their use as receptors in supramolecular host/guest chemistry.

Prof. Nunzio Tuccitto received his PhD in Chemistry in 2007. He is currently an Associate Professor of Physical Chemistry at the University of Catania, Italy. His research is focused on theoretical models governing molecular communication between implantable medical devices, synthesizing molecular messengers based on carbon nanoparticles, and developing bench-top prototypes to test communication. His research activity is also focused on developing nanoparticles for the detection of hazardous gases (e.g., warfare agents) and monitoring of anthropogenic pollutants in the troposphere. He is an expert in big-data processing and machine learning for data processing arising from multi-sensor devices and complex data resulting from mass spectrometry.

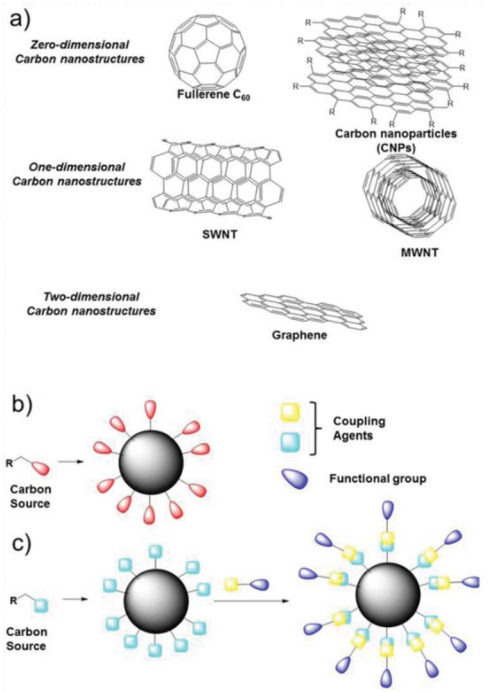

Fig. 1 (a) Classification of carbon nanostructures by their dimensionality, (b) one-pot synthesis of CNPs and (c) covalent functionalization of the external shell.

Since then, CNPs have been prepared using numerous approaches, which can be summarized by grouping them into two large families, *i.e.*, top-down and bottom-up approaches. The former approach involves the decomposition of carbonaceous materials to reach a nanometer size. Bottom-up synthesis involves the decomposition of small carbon-containing molecules until they aggregate to become nanoparticles. In detail, some of the methods used to synthesize CNPs include chemical[18] or electrochemical carbonization,[19] laser ablation,[20] hydrothermal decomposition induced by heat treatment[21] and microwave irradiation.[22,23] The raw materials used vary widely, ranging from simple carbonaceous sources such as citric acid[24] and simple carbohydrates[25] to polymers[26] including biopolymers,[27] and even biomass and food waste.[28]

CNPs exhibit optical absorption peaks primarily in the UV region and partly in the visible. The transitions are generally associated with the π–π* transition of the sp2 conjugated carbon and the n–π* transition of hybridization with heteroatoms of the outer shell containing carboxyl groups or associated with the presence of N, S, P, *etc.* heteroatoms. The adsorption property of CNPs can also be modified through chemical synthesis. In a very elegant approach, Jiang *et al.* developed a rapid hydrothermal method to modulate the bandgap of CNPs, obtaining red, green, and blue luminescent CNPs using three different isomers of phenylenediamines.[29]

The main feature of CNPs is their strong fluorescence, which is often exploited for sensing, having a quantum efficiency in the order of 10% that can reach values of around 80% with respect to the emission of quinine sulfate, depending on the synthetic route, carbon source and doping.[30] In addition, many efforts have been made to improve the quantum yields and biocompatibility of CNPs to obtain useful biosensors; however, to date, these two features are difficult to obtain simultaneously.[31,32] CNPs emit in the visible area and their fluorescence is characterized by two specificities, *i.e.*, it depends on the wavelength of excitation and can be easily modulated by chemical intervention in their core *via* the doping of heteroatoms or passivating and modifying the surface of their outer shell.[33] The mechanism underlying carbon dot fluorescence emissions is attributed to the radiative recombination of excited particles, where the large surface area/particle volume ratio of carbon dots results in the trapping sites being stabilized by surface passivation agents. Dhenadhayalan *et al.* studied the multiple emissive behavior of CNPs prepared from citric acid.[34] The absorption transition of CNPs occurs from both the carbon core in the deep UV region and from surface domains with a broad UV-A region. Upon irradiation of the carbon core, an electron is promoted from the valence band to the conduction band, resulting in the formation of electron and gap charges. In contrast, an n–π* absorption transition occurs above 300 nm in the surface states, involving the lone pair electron present in the functional groups. Therefore, the observed multi-fluorescence bands of C dots mainly come from their carbon core and surface domain. The fluorescence of the carbon core at around 385 nm is due to the radiative recombination of the electron–hole pairs, while the fluorescence in the surface state is caused by the radiative relaxation from the excited state to the ground state. Excitation at around 350 nm and 385 nm results in fluorescence predominantly in the range of 440–490 nm and nm and 500–540 nm, respectively. Surface functional groups can influence fluorescence characterization by electron transfer-based electron pickup and their electron donor behavior.

Fluorescence sensing by carbon nanoparticles can be performed by exploiting mainly three different types of mechanisms, *i.e.*, PET (photoinduced electron transfer), FRET (Foster resonance energy transfer) and IFE (inner filter effect). In the PET mechanism, a generic sensor, constituted by a receptor-spacer-fluorophore, under irradiation undergoes an electron transfer process from the receptor to the fluorophore, thus leading to the "off-mode". In the presence of an analyte bound to the receptor, this electron transfer cannot occur, leading to an enhancement in the emission of the fluorophore ("on-mode").[35] In a FRET sensor, non-radiative energy transfer occurs from the donor fluorophore to the acceptor chromophore. In particular, the donor chromophore shows absorption/emission spectra at higher energy (blue shifted) with respect to the acceptor (red shifted), and the emission spectrum of the donor needs to overlap with the absorption spectrum of the acceptor.[36] The IFE effect is due to the apparent quenching of the emission due to the attenuation of the excitation beam in the cuvette for fluorescence by a radiative energy transfer phenomenon. In particular, in the primary inner effect, the fluorophore excitation or emission energy is adsorbed by a chemical entity, also called an absorber. Thus, the possibility of tuning the absorber or fluorophore concentration will lead to the development of practical sensors for a specific analyte.[37] A

recent interesting review details the photoluminescence mechanisms of CNPs.[38]

Various types of nanoparticles with chemical-dependent luminescence colours have been reported in the literature. CNPs show excitation-dependent emissions, which vary according to the state of surface oxidation.

A relevant report is that by Yuan *et al.*, achieving multiple emission states (red, green and blue emission) by tailoring the surface states with different amino groups.[39] The red emission was related to the fluorophore formed on the surface of CDs. Pyridinic N derived from the synthesis conditions was responsible for the green emission state, and similarly pyrrolic N enhanced the blue emission. Thus, these results confirm the effect of surface groups on fluorescence, which underlies most of the mechanisms involved in sensing. The target analyte is determined because it can selectively influence these surface groups with immediate effects on the emission in terms of intensity (quenching and turn on) or colour.

An interesting optical property of some CNPs is the possibility to be excited with two-photons, having lower (lower) energy with respect to the single excitation photon.[40,41] These CNPs are characterized by lower photobleaching, lower photodamage, and higher tissue penetration.

Furthermore, the possibility to use lower excitation energies allows CNPs having emissions at lower energy values to be obtained (red-emitting), with interesting applications in the preparation of LEDs.[42]

Wen and Yin reported the preparation of excitation-independent CNPs.[43] The authors proposed that the excitation-independent PL mechanism of CNPs is related to the chemistry of their surface groups. The core conjugated π-electron system is responsible for photo-absorption, which is the site where quantum confinement occurs. The surface groups provide a different relaxation of the vibrations due to their excitation-independent emission and large Stokes shift. Li *et al.* reported that the synthesis conditions influence the abundance of surface groups by making the luminescence independent or dependent on the incident radiation.[44] CNPs made from citric acid and urea at 160 °C showed excitation wavelength-independent luminescence, whereas the CNPs synthesised at 240 °C showed excitation wavelength-dependent emission. The excitation wavelength-independent behavior is due to the presence of a single surface state, whereas for CDs made at 240 °C, when the excitation energy is greater than the energy gap, their emission is controlled by the surface state transitions.

Presently, CNPs can be characterized using many instrumental techniques to obtain information about their elemental composition, morphology, topography, and size distribution. In particular, some microscopic methods can be used to obtain morphological information, such as atomic force microscopy (AFM), transmission electron microscopy (TEM) and scanning electron microscopy (SEM). In addition, dynamic light scattering (DLS) measurements lead to information about particle size.[45] Also mass spectroscopy, including electrospray ionization quadrupole time-of-flight tandem mass spectrometry (ESIQ-TOF-MS/MS)[46] and matrix-assisted laser desorption/ionization time-of-flight mass spectrometry (MALDI-TOF MS),[47] can be used to obtain information about the composition of nanoparticles. In addition, spectroscopic methods, such as photoluminescence UV-Vis, IR and Raman spectroscopy, are usually employed to obtain spectral information (*vide infra*). Energy dispersive X-ray spectroscopy (EDX) can be also used to obtain elemental composition and determine the purity of nanoparticles.[48] Furthermore, covalent functionalization of their external shell can be confirmed by nuclear magnetic resonance spectroscopy (NMR) experiments[49,50] and X-ray photoelectron spectroscopy (XPS) analyses.[51]

CNPs for chemical sensing

CNPs have been widely employed for the chemical sensing of pH, important biological active molecules, other metal nanoparticles, hydrogen peroxide, VOCs, nitrites, explosives, sugars, thiols and other natural or synthetic molecules. In general, sensing leads to the quenching of the emission of CNPs due to their interactions with the analyte. Furthermore, in some cases, the sensor is composed of hybrid nanoparticles, which are also based on some metal-nanoparticles.

Table 1 presents a summary of the chemical sensing applications of carbon nanoparticles, highlighting their carbon source, fluorescence mechanism for sensing and important parameters such as linearity range and limit of detection.

pH

The possibility to monitor the pH value in the cellular microenvironment is of particular interest in many fields, such as bioimaging and diagnosis. Accordingly, the size of pH probes must be in the range of nanometers for them to be internalized in the selected intracellular compartment.

Du and co-workers developed a ratiometric sensor for intracellular pH detection based on FRET by covalently binding fluorescein isothiocyanate (FITC), a pH-sensitive fluorescent dye, to CNPs.[52] In this FRET system, the CNPs act as the donor and FITC as the acceptor (Fig. 2). Due to the important characteristics of the designed sensor, such as low cytotoxicity, good cell permeability and high reversibility, it was used to map the pH gradient in living cells.

In addition, Ouyang and co-workers synthesized N-doped fluorescent CNPs, which were characterized by a high quantum yield (63.2%) and could detect pH changes in solution and in the intracellular environment.[53] The emission intensity of these nanoparticles showed a good linearity ($R^2 = 0.995$) with an increase in pH in a lower pH range (3.47–5.10) with respect to the previous example. Notably, these nanosensors could also be recovered and reused at least 11 times in cell experiments (Fig. 3).

Similar results were obtained by Shuang and co-workers using orange fluorescent CNPs prepared from 5-amino salicylic acid and hydrothermal treatment.[54] These CNPs showed a linear response between 5.2 and 6.8, with good linearity ($R^2 = 0.994$). Also in this case, this sensor was tested for intracellular measurements.

Table 1 Summary of chemical sensing by CNPs

Sensing	Carbon source	Mechanism of fluorescence detection	Linearity	LOD	Ref.
pH	Acrylic acid, ethylenediamine	FRET	pH 4.5–6		*Nanotechnology*, 2013, **24**, 365101 (ref. 52)
	Citric acid, aniline	Quenching	pH 3.47–5.10		*Talanta*, 2018, **186**, 80 (ref. 53)
	5-Amino salicylic acid	Quenching	pH 5.2–6.8		*Talanta*, 2019, **196**, 109 (ref. 54)
	Citric acid	Quenching	pH 6–10		*ACS Appl. Nano Mater.*, 2021, **4**, 9738 (ref. 56)
N-based compounds	Acetic acid	FRET		3 ppm	*Sens. Actuators, B*, 2016, **225**, 522 (ref. 57)
	Food grade honey	Enhancement	4.9–38 nM	2.3 nM	*J. Fluoresc.*, 2016, **26**, 129 (ref. 58)
H_2O_2	Carbohydrates	Enhancement	20–20.000 mM	5 μM	*Talanta*, 2015, **144**, 1308 (ref. 59)
	Citric acid, ethylenediamine	PET	0–2 mM	84 nM	*Chem. Commun.*, 2015, **51**, 15574 (ref. 60)
	Glucosamide hydrochloride	Enhancement	0.1–10 mM	87 nM	*J. Mater. Sci.*, 2020, **55**, 16928 (ref. 61)
VOC	pCN-TPA	ICT			*RSC Adv.*, 2016, **6**, 83501 (ref. 62)
Explosives	Ammonium citrate	FRET	0–20 mM	0.25 mM	*J. Mater. Chem. A*, 2016, **4**, 4161 (ref. 63)
	Activated carbon	Quenching	10–600 mM	2 ppm	*Carbon*, 2016, **106**, 171 (ref. 64)
	Carbon nanopowder	Quenching – CT			*Inorg. Chim. Acta*, 2017, **468**, 300 (ref. 65)
S-based compounds	Histidine	Quenching	0–2 mM	0.036 μM	*Analyst*, 2015, **140**, 8157 (ref. 66)
	Histidine and citrate	FRET	0–50 mM	18 nM	*Analyst*, 2015, **140**, 6711 (ref. 67)
	Tris	FRET	1–1900 nM	0.4 nM	*Sens. Actuators, B*, 2018, **264**, 404 (ref. 69)
	Silkworm droppings	Enhancement	1–1000 μM	0.13 μM	*Nanomaterials*, 2018, **8**, 443 (ref. 70)
	Citric acid, cysteine	Enhancement	1–10 mM	1 mM	*Sens. Actuators, B*, 2018, **266**, 553 (ref. 71)
	Asparagine	Enhancement	0.01–0.9 mM	0.01 mM	*Anal. Bioanal. Chem.*, 2019, **411**, 2597 (ref. 68)
Glucose	CCl_4, ethylenediamine	n.d.	40 μM to 20 mM	40 μM	*Electrochim. Acta*, 2013, **95**, 260 (ref. 72)
	Phenylboronic acid	Quenching	9–900 μM	1.5 mM	*Anal. Chem.*, 2014, **86**, 5323 (ref. 73)
	Citric acid, ethylenediamine	Enhancement	2.0–400 μM	0.67 μM	*Sens. Actuators, B*, 2018, **265**, 310 (ref. 74)
	Lignite	Quenching	1–10 mM	0.125 mM	*Sci. Rep.*, 2018, **8**, 13891 (ref. 75)
Drugs	Ascorbic acid	Quenching	0.5–3 μM (blue channel) 0.1–3 μM (yellow channel)	0.037 mM	*Colloids Surf., B*, 2018, **162**, 212 (ref. 76)
	Honey	Quenching	100 nm to 1000 mM	6 nM	*Mater. Today Bio*, 2021, **12**, 100168 (ref. 77)
	m-Phenylenediamine, DAP	Enhancement	0.005–0.16 μM	2 nM	*Sens. Actuators, B*, 2018, **274**, 296 (ref. 78)
	Glucose	Enhancement	0.8–80 μM	0.55 μM	*Nanoscale*, 2019, **11**, 18845 (ref. 79)
	Riboflavin	Enhancement	0–100 mg mL^{-1}	250 ng mL^{-1}	*Sens. Actuators, B*, 2019, **301**, 127149 (ref. 80)
	Eucalyptus twigs, ammonium chloride	Quenching	0.25–2 μM,	200 nM	*ACS Omega*, 2020, **5**, 19905 (ref. 81)
	Citric acid	Quenching	1–100 nM	0.39 ppt	*ACS Appl. Nano Mater.*, 2020, **3**, 8182 (ref. 82)
		FRET	0–40 mM	0.41 μM	*Spectrochim. Acta Mol. Biomol. Spectrosc.*, 2021, **246**, 118947 (ref. 84)
	Citric acid	Quenching	0–1.5 mg mL^{-1}	0.1 mg mL^{-1}	*ACS Appl. Nano Mater.*, 2021, **4**, 6250 (ref. 85)
	Citric acid	Quenching	0–1 mM	57 nM	*Anal. Chim. Acta*, 2021, **1165**, 338513 (ref. 86)
	Citric acid, ammonia sulphate	Quenching	0.05–4 mM	0.003 mM	*Spectrochim. Acta Mol. Biomol. Spectrosc.*, 2021, **262**, 120148 (ref. 87)
	Citric acid, melamine	Enhancement	0.005–0.1 mg L^{-1}	2.32 mg L^{-1}	*Spetrochimica Acta, Part A*, 2021, **250**, 119384 (ref. 89)

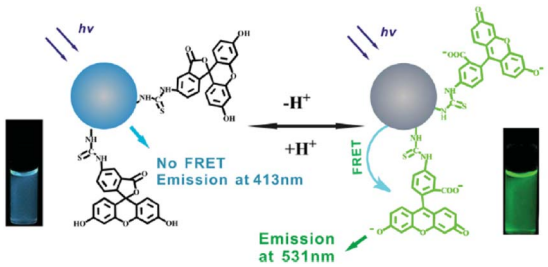

Fig. 2 Schematic representation of pH sensing by FRET mechanism (reproduced with permission from *Nanotechnology*, 2013, **24**, 365101, Copyright 2013, IOP Science).

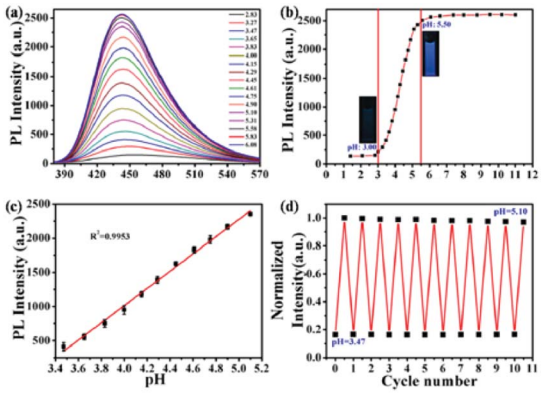

Fig. 3 (a) Fluorescence spectra at different pH values, (b) plot of the emissions during titration, (c) liner response of the CNPs to pH value, and (d) recovery test (adapted with permission from *Talanta*, 2018, **186**, 80–87, Copyright 2018, Elsevier).

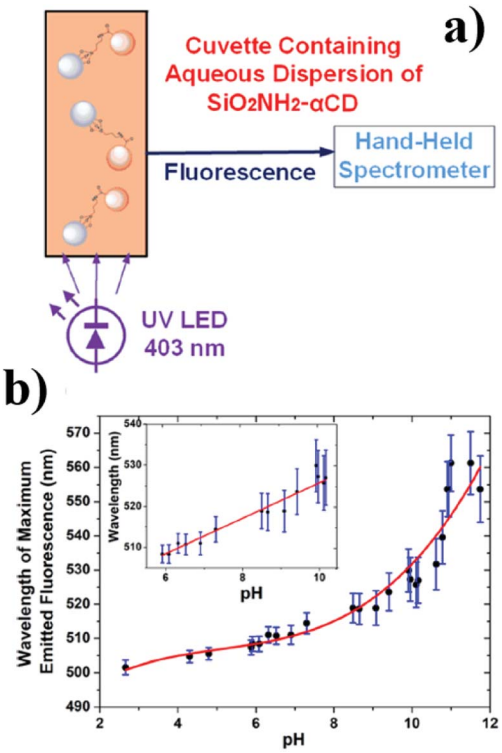

Fig. 4 (a) Schematic representation of the device and (b) emission as a function of pH (reproduced with permission from *ACS Appl. Nano Mater.*, 2021, **4**, 9738–9751, Copyright 2021, the American Chemical Society).

In the same context, Pan and co-workers exploited the ability of yttrium-doped CNPs to detect pH changes for the detection pathogens.[55] These nanoparticles showed a high dispersion in water, and consequently they were uniformly included in a 3D agarose gelatinous matrix without the formation of aggregates. This sensor could detect pH variations by fluorescence emission changes. Bacterial growth was detected in saliva samples using a small amount of sample (100 μL) in almost real time (25 min).

Recently, Prato and co-workers reported the implementation of their other work, obtaining hybrid nanoparticles based on silica and carbon in an agarose matrix, which could detect pH after LED irradiation.[56] In particular, silica nanoparticles containing amino groups were covalently bounded with CNPs, exploiting the free carboxy groups *via* stable amide bond formation. These hybrid nanoparticles were introduced into a waveguide, thus obtaining a practical optical sensor (Fig. 4). This sensor was stable and reversible, and in addition showed a high sensitivity 5.61 nm per (pH unit) and a linear response in the pH range of 6–10.

Nitrogen-based compounds

The qualitative and quantitative determination of nitrogen compounds are essential for environmental, industrial, and biomedical purposes. Thus, to achieve this target, several instrumental and colorimetric methods have been developed to detect N-based compounds in solution and in the vapour phase.

Cyriac and co-worker reported fluorescent CNPs for the selective and sensitive detection of ammonia species *via* a FRET mechanism, exploiting sodium rhodizonate as the receptor molecule.[57] The fluorescence sensing mechanism is FRET from the CNPs to sodium rhodizonate, activated in the presence of ammonia, leading to quenching of the fluorescence of the CNPs, with an LOD of 3 ppm. In addition, ammonia vapors were detected by cotton fibers adsorbed with the sensor solution. This presented a low-cost, reversible, selective and stable system for the detection of oxides of nitrogen and common organic solvents.

Another possible application of nanoparticles as fluorescent sensors for nitrogen-based compounds was reported by Kumar and co-workers.[58] They synthesized PEG6000-coated carbon nanoparticles for the determination of nitrites in different types of matrices such as milk, borewell water and soil samples. The interaction with NO_2^- causes a fluorescence enhancement, which can be monitored to analyze the presence of the analyte. The obtained sensor demonstrated a linear response in the range of 4.9×10^{-9} M to 3.8×10^{-8} M, a detection limit of 2.3×10^{-9} M, and good selectivity.

H_2O_2

The real-time monitoring of hydrogen peroxide levels is of primary interest in many fields, such as the biological and

environmental fields, due to their correlation with cellular oxidative stress, as well as the use of H_2O_2 in many industrial processes. Bendicho and co-workers synthesized fluorescent CNPs by exploiting the UV irradiation of carbohydrates.[59] The obtained carbon nanoparticles could be used as fluorescent sensors for the detection of hydrogen peroxide and antioxidant agents, such as ascorbic acid and glutathione. In fact, the presence of hydrogen peroxide leads to a decrease in the dimensions of CNPs and an increase in their fluorescence emission, while antioxidants inhibit the action of hydrogen peroxide, leading to a decrease in the emission of the CNPs. A detection limit of 5 μM was observed for hydrogen peroxide, with a linearity in the wide range of 20–20.000 mM. Notably, this sensor was used for the detection of hydrogen peroxide in solutions for cleaning contact lenses.

Zhang and co-workers designed a PET-based sensor for the detection of hydrogen peroxide using fluorescent CNPs.[60] These nanoparticles were obtained starting from citric acid and ethylenediamine as precursors, and subsequent surface functionalization with 2-(diphenylphosphino) ethylamine. The CNPs functionalized with diphenylphosphine possessed an acceptor and donor moiety for the PET mechanism, where the presence of hydrogen peroxide hinders the PET process due to the oxidation of the phosphine portion (Fig. 5). This system was sensitive, selective, and useable in a wide pH range, with a detection limit of 84 nM.

Recently, Chen and co-workers reported a hybrid nanomaterial based on AgNPs and CNPs for the detection of hydrogen peroxide.[61] This system showed a linear response in the range of 0.1–10 mM, with a detection limit of 0.087 mM. This system was employed for the colorimetric detection of water peroxide in urine and lake water. Furthermore, the fluorescence turn-on observed in the presence of H_2O_2 led to the possibility of this molecule also being able to detect H_2O_2 in human breast cancer (MCF-7) cells.

Volatile organic compounds (VOCs)

The presence of VOCs in the atmosphere due to human activity is related to many respiratory disorders. Accordingly, the possibility to detect VOC levels with high efficiency, accuracy and selectivity is of huge interest for human safety.

Xie and co-workers synthesized CNPs for the detection of VOCs.[62] In particular, they adsorbed a solution of CNPs on reactive paper, thus obtaining a solid sensor that could detect, through a variation in fluorescence, the presence of VOCs instantly, similar to optical noise. Materials with solvatochromic characteristics were exploited to determine these analytes quickly and sensitively. Amphiphilic CDs were synthesized from (*Z*)-4-(2-cyano-2-(40-(diphenylamino)-[1,10-biphenyl]-4-yl)-vinyl) benzonitrile, PEG2k and pCN-TPA, which were chosen for their intramolecular charge-transfer properties. Based this type of synthesis and functionalization, the CNPs possessed different luminescence behaviors in different solvents and showed, for each solvent, a typical excitation-dependent feature (Fig. 6). These sensors were shown to be reversible, sensitive and selective to various VOCs.

Explosives

The fast, smart, sensitive and selective detection of explosives has received increasing attention due to their implications in homeland security, global demining and environmental safety. Traditional analytical techniques are based on large instruments, such as HPLC and GC-MS, and thus the facile detection of these organic substance is of particular interest.

In this context, Lei and co-workers reported the microwave-assisted synthesis of n-doped CNPs starting from a single precursor, ammonium citrate dibasic, thus obtaining nanosensors that could selectively detect picric acid.[63] In fact, in contrast to other nitroaromatic explosive compounds, the interaction with picric acid led to quenching of the fluorescence signal of the CNPs. This is due to the greater synergistic effects such as acid–base interactions between the NPs and analyte, and also the presence of the FRET mechanism from the excited state of the CNPs to the picric acid, thus leading to the sensitive detection of the explosive, with a calculated detection limit of 0.25 mM and a linear response under 20 mM. The selectivity was with evaluated also other nitro-compounds.

Algarra and co-workers reported fluorescent nanosensors for the detection of 4-chloro-2,6-dinitroaniline, a widespread component of explosives.[64] These sensors were based on carbon nanoparticles, which were synthesized *via* the oxidation of activated carbon in water and functionalized with amino groups using PAMAM-NH_2 dendrimer. The interaction between the sensor and analyte, in addition to causing quenching of the fluorescence at 465 nm, also led to the appearance of a new band at 507 nm, which highlighted the formation of a Meisenheimer complex. Therefore, the linearity of the response was in the range of 1×10^{-5} M to 6×10^{-4} M, with a good sensitivity of 2 ppm.

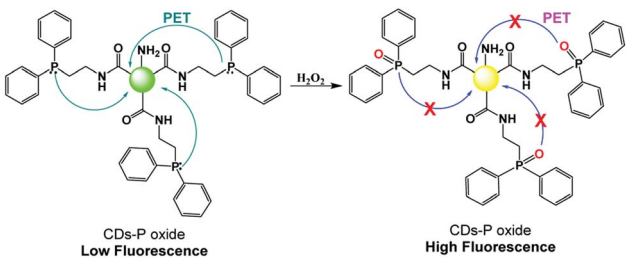

Fig. 5 Mechanism of H_2O_2 sensing by fluorescent CNPs functionalized with 2-(diphenylphosphino) ethylamine.

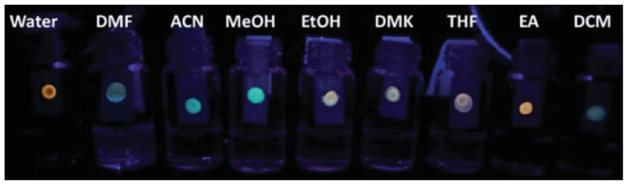

Fig. 6 Images of paper sensor strip containing CNPs after exposure to the vapor of solvents taken under a UV lamp (365 nm) (reproduced with permission from *RSC Adv.*, 2016, 6, 83501–83504, Copyright 2016, The Royal Society of Chemistry).

In 2017, Sun and co-workers functionalized carbon nanoparticles with 2,2′-(ethylenedioxy)bis(ethylamine) (EDA) to obtain fluorescent sensors that could detect nitrotoluene molecules.[65] The underlying recognition mechanism involves fluorescence quenching caused by the charge transfer interactions between the probe and analyte. These examples demonstrate the high versatility of carbon nanoparticles to detect different typologies of explosives, depending on their external functionalization.

Sulphur-based compounds

Thiols and other S-based compounds play crucial roles in many physiological functions and can be found in numerous biologically significant molecules. Alterations in the concentrations of these molecules can be related to many disorders, such as Alzheimer's disease and osteoporosis.

Yang and co-workers proposed a new colorimetric and fluorimetric sensor for the detection of the thiocyanate ion (SCN^-).[66] This sensor consisted of amino-functionalized CNPs, which by means of Au–N interaction, were adsorbed on the surface of citrate-stabilized gold nanoparticles (Au-NPs), thus leading to the aggregation of the nanoparticles and quenching of the fluorescence emission. SCN^- ions preferentially bind to the surface of the gold nanoparticles, and consequently the interaction between the gold nanoparticles and the carbon dots is disrupted. An increase in the emission and a color change, from blue to red were observed. In particular, it was observed that a color change perceptible to the naked eye occurred at an SCN^- concentration of 1 μM, and furthermore a detection limit as low as 0.036 μM was obtained.

Chen and co-workers designed a double-emission hybrid nanosensor for the detection of the sulphide anion, using carbon nanoparticles synthesized from histidine and trisodium citrate dihydrate.[67] The sensing mechanism is due to FRET from the CNPs to the covalently bound gold nanoparticles. The detection of S^{2-} is due to the formation of the Au_2S species, thus leading to the destruction of the FRET process (see Fig. 7). This probe allowed the detection of S^{2-} in a sensitive, selective and rapid way, with a detection limit of 18 nM and a linear response under 50 mM. Notably, this system could detect the S^{2-} anion in real samples, such as hot spring water.

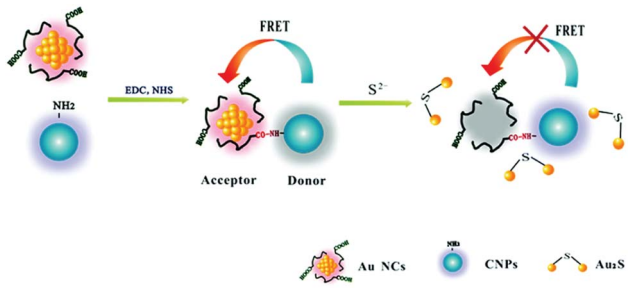

Fig. 7 Sensing mechanism of S^{2-} based on CNPs and AuNCs (reproduced with permission from *Analyst*, 2015, **140**, 6711–6719, Copyright 2015, The Royal Society of Chemistry).

In the same context, John and co-worker reported the preparation of hybrid nanomaterials based on silver and carbon nanoparticles for the colorimetric and fluorescence detection of sulfide ions.[68] In particular, CNPs were capped on AgNPs, acting as fluorescent and colorimetric probes, respectively. The presence of 0.1 μM of S^{2-} decreased the absorption intensity of the nanocomposite, changing its color from yellow to colorless, but increasing its fluorescence emission intensity. The linear range observed was 0.01–0.9 mM, with an LOD of 0.01 mM. This behavior is due to the formation of Ag_2S. The goals of this nanosensor were the possibility to detect H_2S in real water samples, easy analysis and good selectivity.

Wang and co-workers reported a fluorescent nanoprobe for the detection of hydrogen sulfide (H_2S).[69] This fluorescent sensor was based on carbon nanoparticles modified with silver nanoparticles (AgNPs). This hybrid nanosystem showed a linear detection response to H_2S from 1 to 1900 nM, with the detection limit of 0.4 nM. The CNPs were prepared using (tris(hydroxymethyl)-aminomethane). The binding between carbon and silver nanoparticles led to fluorescence quenching through the FRET mechanism. The fluorescence of the single nanoparticles could be efficiently recovered by H_2S, thus giving an emission signal due to Ag–S bond formation. The sensing mechanism was supported by DFT/TD-DFT experiments. In addition, sensing of H_2S in the cerebral system was also performed with this sensor.

Cao and co-workers used silkworm droppings as the starting material to obtain fluorescent nitrogen-doped CNPs (N-CNPs) *via* hydrothermal treatment.[70] These N-CNPs exhibited good optical properties, showing bright blue emission under ultraviolet excitation and good water solubility, and were used for the detection of Fe^{3+} *via* the "on–off–on" mechanism. This mechanism is due to the presence of Fe^{3+} ions, which led to the quenching of the nanoparticle emission, with a detection limit of 0.20 μM in the linear range of 1–500 μM. Subsequently, the introduction of biothiols led to the recovery of fluorescence, resulting in an "off–on" process. This sensor was also applied for the quantification of glutathione (GSH) in fetal calf serum samples, with an LOD of 0.13 μM in the linear range of 1–1000 μM.

Yu and co-workers reported the first array based on multichannel fluorescent CNPs with metal ions for the sensing of thiols.[71] The functional groups on the surface of the CNPs interact with metal ions, leading to the aggregation of the CNPs, thus quenching the fluorescence of the nanoparticles themselves. The seven thiols used showed a different affinity for metal ions, and consequently the fluorescence was modified by the presence of thiols. According to these responses, the identity of thiols was detected by linear distinction of the assay (LDA), at a low concentration of 1.0 μM (Fig. 8). This sensor could identify 42 thiols in fetal bovine serum and urine.

Glucose

The correlation of the glucose levels in blood with diabetes is well-known. Thus, the possibility to monitor the blood glucose level is essential for diabetic patients. The available kits to

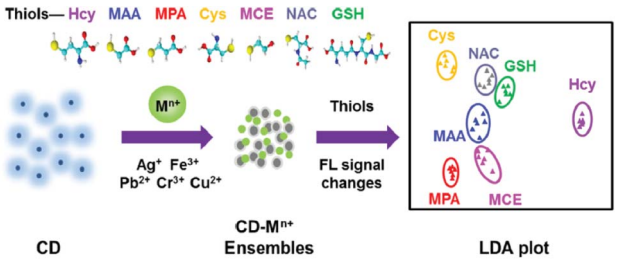

Fig. 8 Schematic representation of the fluorescent sensor array for the detection and discrimination of thiols (adapted with permission from *Sens. Actuators, B*, 2018, **266**, 553–560, Copyright 2018, Science Direct).

control glucose levels in the blood are based on electrochemical techniques, having enzymes as receptors. However, the possibility to tune to fluorescent sensors should improve their sensibility and response time. In this context, Sun and co-workers demonstrated that one of the applications of photoluminescent carbon nanoparticles is in the construction of a glucose biosensor.[72] In fact, CNPs resulted in the colloidal stability of the rGO (reduced graphene oxide) dispersion by acting as stabilizing agents for the reduced graphene oxide (GO) and leading to the formation of CNPs–rGO; moreover, in the presence of glucose oxidase (GOD), the attractive electrostatic interactions lead to the formation of the GOD–CND–rGO hybrid. This sensor was obtained by depositing the hybrid system on a glass carbon electrode, obtaining a linearity of detection from 40 μM to 20 mM and a limit of detection of 40 μM. This sensor was used for the detection of blood serum glucose.

A new type of fluorescent sensor based on CNPs was synthesized using phenylboronic acid as a precursor by Xia and coworker.[73] The obtained CNPs could be used for the detection of glucose because the *cis*-diol groups of glucose can covalently bind to the boronic acid moieties on the surface of the CNPs, leading to an assembly of the latter, and consequently extinction of the fluorescence. A detection limit of 1.5 μM and an interval in which the fluorescence quenching is linear from 9 to 900 μM were observed. With this type of sensor, glucose can be determined in the presence of its analogues and potential interfering substances present in the blood, and thus the sensor can be used for the detection of blood glucose in human serum.

Rao and co-workers developed a dual-signal fluorometric and colorimetric sensor for the rapid, sensitive, and selective detection of glucose, consisting of bimetallic Au@Ag core–shell nanoparticles (Au@AgNPs) and carbon nanoparticles.[74] These Au@AgNPs were mixed with a CNP solution, which were synthesized *via* the hydrothermal method. The emission of the CNPs was quenched by the silver nanoparticles. However, the presence of H_2O_2 restored the fluorescence of the CNPs due to the oxidation of the gold external shell by the enzymatic reaction in the presence of glucose. This led to a color change from yellow-orange to pink, which was correlated with the glucose concentration. This linearity was in the range of 2.0–400 μM, with a detection limit of 0.67 μM. This method was also applied for the sensing of glucose in blood samples.

Similarly, Manoi B. and co-workers reported the preparation of CNPs and graphene oxide layers starting from lignite as a precursor for glucose sensing.[75] In particular, in this synthesis, they used a top-down approach. Carbon nanocrystallites contained in lignite were oxidized into carbon nanoparticles and graphene sheets, showing fluorescence in the visible region depending on their size and chemical structure. These nanosensors showed a linear fluorescence response in the presence of glucose. Therefore, these fluorescent CNPs show good selectivity for glucose, with a detection limit of 0.125 mM.

Drugs

Drug detection is mainly performed using instrumental techniques (HPLC and GC-MS), which require complex analytical protocols, long-time and high-cost analysis. Thus, the development of fluorescent sensors for this purpose should lead to faster and easier analysis.

Qu and co-workers reported a fluorescence strategy to detect dopamine and tyrosinase activity by synthesizing dual-emitting CNPs, which could emit in blue and yellow.[76] The presence of gold nanoparticles led to the quenching of their emission, which was recovered by the presence of dopamine, which interacted with the AuNPs, leading to the formation of aggregates. The authors demonstrated high selectivity for dopamine in the concentration range of 0.5–3 μM for the blue channel and 0.1–3 μM for the yellow channel. In addition, this system could be exploited to detect dopamine and tyrosinase activity simultaneously due to the ability of tyrosinase to oxidize dopamine into dopaquinone, which does not interact with AuNPs. This method was also used to detect dopamine in plasma.

Dopamine was recently recognized with higher sensibility by Yun and co-workers using CNPs obtained from honey.[77] In particular, the presence of dopamine led to a quenching of the emission due to the redox reaction between dopamine and CNP

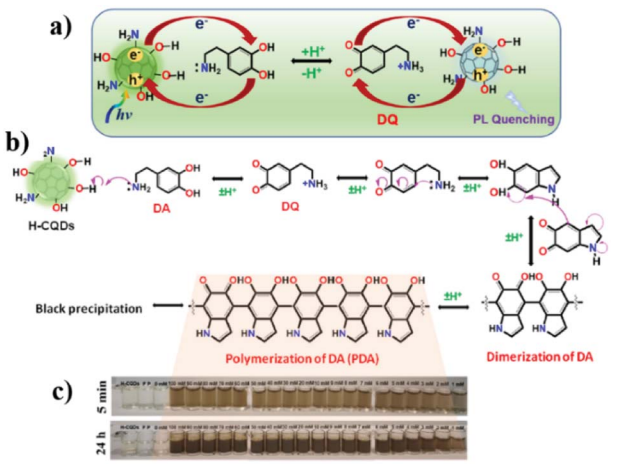

Fig. 9 (a) Redox reaction between CNPs and dopamine, (b) proposed mechanism of dopamine polymerization and (c) color change of CNP solution with different dopamine concentrations after 5 min and 24 h (adapted with permission from *Mater. Today Bio*, 2021, **12**, 100168, Copyright 2021, Elsevier).

(Fig. 9a). This system showed a linear response in the range of 100 nm to 1000 mM, with a calculated LOD of 6 nM.

Notably, this detection could be monitored using a simple smartphone due to the progressive change in the color of the solution (from pale yellow to dark brown in *ca.* 24 h, Fig. 9c) due to the formation of polydopamine (Fig. 9b).

Hou and co-workers reported the use of N,P-doped carbon nanoparticles (N,P-CNPs) and gold nanoparticles (AuNPs) for the sensing of carbendazim, a wide-spectrum fungicide, *via* the FRET mechanism.[78]

The CNPs were prepared *via* a one-pot hydrothermal reaction using diethylenetriaminepenta-methylenephosphonic acid (DAP) and *m*-phenylenediamine as the N and P sources, respectively, showing an emission at 512 nm, which could be quenched by the presence AuNPs. After the introduction of carbendazim in the N,P-CNP solutions, the intensity of the fluorescence increased due to the interaction between carbendazim and the AuNPs. The authors reported a linear range of 0.005 μM to 0.16 μM, with a calculated detection limit of 0.002 μM, and good selectivity.

Glutathione (GSH) was well recognized using a multifunctional nanosensor by Shuang and co-workers.[79] In particular, the hybrid nanosensor was realized by integrating CNPs, silver nanoparticles (AgNPs) and MnO_2. The CNP@MnO_2 nanocomposite was obtained *via* the deposition of MnO_2 on CNPs. AgNPs were anchored on CNP@MnO_2 by electrostatic interaction. The presence of MnO_2 led to quenching of the emission, but the addition of GSH increased the fluorescence due to its ability to oxidize MnO_2 (Fig. 10). This turn-on sensor could also be used for *in vivo* measurements, with a linear range of 0.8–80 μM and a detection limit of 0.55 μM.

S. V. Carneiro and co-workers developed a hybrid nanomaterial based on silver and carbon nanoparticles for the fluorescent detection of pesticides in foods.[80] The fluorescence of the CNPs (360 nm) was quenched by the AgNPs *via* the FRET mechanism. This probe could discriminate many pesticides, such as propanil, parathion, dimethoate, chlorpyrifos, and pirimicarb in real samples of rice, carrot, orange, and pepper. The results were analyzed by LDA analysis, thus obtaining diagnostic response patterns as a function of pesticide composition and concentration.

Nag and co-workers reported the preparation of light-blue CNPs for the detection of Brilliant Blue FCF (BB), a toxic synthetic food colorant.[81] These nanoparticles were obtained from dry *Eucalyptus* twigs and ammonium chloride as starting materials. Different emissive nanoparticles were obtained after filtration and washing. The presence of BB led to quenching of the emission, with a limit of detection of 200 nM, in the analysis of real food samples. This nanosensor was also tested in human cell lines (MDA-MB-231), demonstrating low toxicity.

Recently, our research group developed new CNPs covalently functionalized with ethanolamine arms[82] for the efficient, selective, sensitive, and reversible detection of ppm levels of chemical warfare agents (CWAs), both in water and the air, using a supramolecular approach.[83] These arms interacted with a CWA simulant (DMMP) *via* the formation of multiple hydrogen bonds (Fig. 11), which guaranteed high selectivity and sensitivity (sub-ppt). In addition, the fluorescence properties of the CNPs led to the possibility of using a smartphone to detect the presence of the CWA simulant. Notably, this sensor could be reused at least 7 times.

Song and co-workers reported the synthesis of CNPs for the sensing of oxytetracycline (OTC) *via* the FRET mechanism.[84] The surface of the blue fluorescent CNPs, covered by amine, carboxyl and hydroxyl groups, interacted with OTC *via* multiple hydrogen bonds and π–π stacking interactions, reducing their distance to a few nanometers. Thus, the overlap between the absorption spectrum of OTC and the emission spectrum of CNPs occurred, increasing the energy transfer from the CNPs to OTC. In this way, the blue emission of the CNPs was quenched and a new green emission (505 nm) was detected. This sensor showed good selectivity and sensitivity to OTC, with a limit of detection of 0.41 μM. In addition, these nanoparticles were

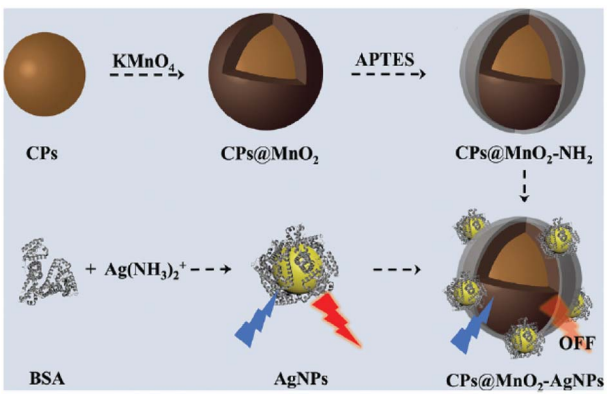

Fig. 10 Schematic representation of the synthesis of CNPs@MnO_2 (reproduced with permission from *Nanoscale*, 2019, **11**, 18845–18853, Copyright 2019, The Royal Society of Chemistry).

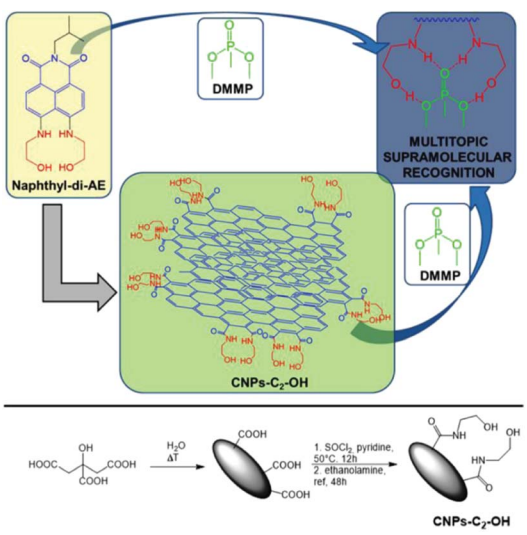

Fig. 11 Representation of CNPs-C2-OH and DMMP chelation mechanism. Bottom: Synthesis of CNPs-C2-OH (reproduced with permission from *ACS Appl. Nano Mater.*, 2020, **3**, 8182–8191, Copyright 2020, the American Chemical Society).

utilized for real sample analyses in river water, tap water, mineral water, milk, and pork.

Recently, Tuccitto and co-workers reported the preparation of fluorescent CNPs as a fluorescent sensor for the selective detection of amino acids.[85] In particular, the analysis of the excitation–emission bidimensional maps showed that the CNP emission properties were strictly related to the interactions between the nanoparticle surface and the amino acids (Fig. 12). Exploiting the machine learning approach based on artificial neural networks, it was possible to discriminate different amino acids.

Recently, Jung and co-workers reported the use of CNPs covalently functionalized with glutathione (GSH-CNPs) for the sensing of levodopa.[86] The interaction between levodopa and the nanosensor, in alkaline condition, led to quenching of its emission due to the conversion of levodopa into dopaquinone, which interacts with the thiol groups of GSH-CNPs. A linear response was observed under 1 mM, with a limit of detection of 0.057 mM.

Shahlaei and co-workers reported the synthesis of a hybrid nanosystem based on fluorescent silver–carbon nanoparticles obtained from a mixture of citric acid, ammonia sulphate and different metals *via* the hydrothermal method for the detection of gemcitabine, a well-known chemotherapeutic agent.[87] The interaction between the nanosensor and gemcitabine led to the quenching of its emission due to the PET mechanism. A linear response was reported between 0.003 and 0.1 mM, and a limit of detection of 0.002 mM. Notably, gemcitabine was also detected in real samples (human plasma and urine).

Chen and co-workers reported a fluorescent sensor based on CNPs as a probe and a molecular imprinted polymer to accommodate and recognize naproxen, one of the most used drugs for the treatment of inflammation, fever, and pain.[88] In particular, the presence of the analyte led to a decrease in the emission intensity, with a limit of detection of 0.03 mM and a linear response between 0.05 and 4 mM. The authors tested the sensing application in real samples, using tap, river water, and simulative human urine.

Gao and co-workers reported on an ultrasensitive and rapid "turn-on" fluorescence device based on nitrogen-doped CNPs and AuNPs for sensing metformin hydrochloride (MET) in urine biological fluids.[89] The hybrid nanosystem was assembled *via* electrostatic interactions between the terminal amino groups of the CNPs and the positive charge of the AuNPs (Fig. 13). In this condition, the emission of the CNPs is quenched; however, after the addition of MET (positively charged), these electrostatic interactions are broken, restoring the starting CNPs, thus leading to a significant increase in their emission. This prototype showed many features, such as sensitivity, low cost and precision. In fact, MET could be detected with a linear range (0.005–0.1 mg L^{-1}) and limit of detection of 2.32 mg L^{-1}, which is much lower than that with other common techniques.

CNPs for ion sensing

Heavy metals, under specific concentrations, are essential components for normal metabolism. However, the presence of an excess of these metal ions leads severe disorders. Consequently, the qualitative and quantitative determination of these

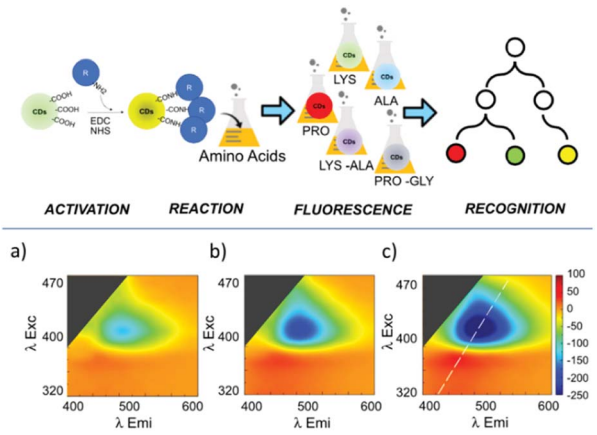

Fig. 12 (a) Representation of amino acid recognition based on the effect on the CNPs fluorescence coupled with machine learning capabilities. (b) 2D-maps of fluorescence difference after surface functionalization of activated CDs with GLY at various concentrations (reproduced with permission from *ACS Appl. Nano Mater.*, 2021, **4**, 6250, Copyright 2021, The American Chemical Society).

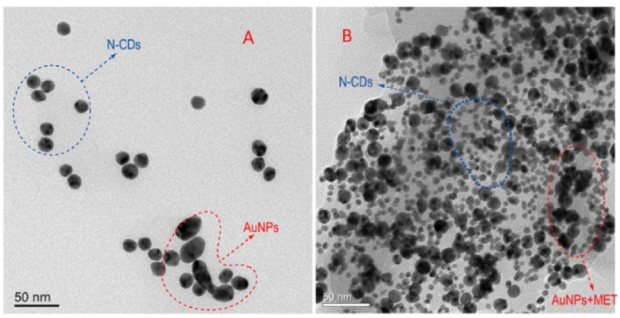

Fig. 13 TEM images of N-CNPs/AuNPs without (A) and with MET (B). (Reproduced with permission from *Spectrochimica Acta, Part A*, 2021, **250**, 119384, Copyright 2021, Elsevier).

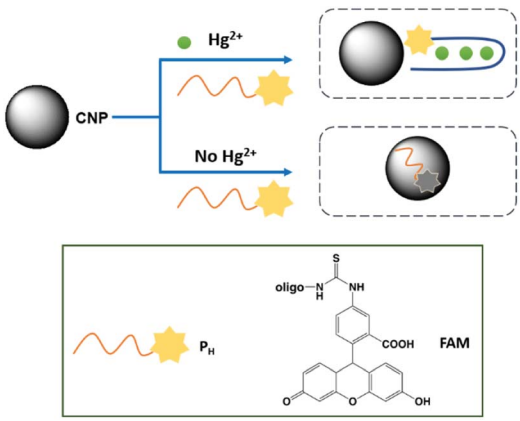

Fig. 14 Schematic representation of Hg^{2+} sensing mechanism by CNPs based on conformational change of DNA strand.

Table 2 Summary of ion sensing by CNPs

Sensing	Carbon source	Mechanism of fluorescence detection	Linearity	LOD	Ref.
Hg	Candle soot	Enhancement	10–250 nM	10 nM	*Biosens. Bioelectron.*, 2011, **26**, 4656 (ref. 90)
	Pomelo peel	Quenching	5–10 nM 0.5–40 μM	0.23 nM	*Anal. Chem.*, 2012, **84**, 5351 (ref. 91)
	Flour	Quenching	0.5–10 nM	0.5 nM	*Sens. Actuators, B*, 2013, **184**, 156 (ref. 92)
	Sweet potatoes	Quenching	n.d.	1 nM	*J. Nanoparticle Res.*, 2013, **15**, 1344 (ref. 93)
	Melamine, trisodium citrate dihydrate	Quenching	0–6 mM	42 nM	*ACS Appl. Mater. Interfaces*, 2014, **6**, 21270 (ref. 94)
	Coconut milk	Quenching	30–50 nM	16.5 nM	*J. Lumin.*, 2015, **161**, 117 (ref. 95)
	Citric acid, $(NH_4)_3PO_4$	Quenching	6 nM to 12 mM	2.3 nM	*RSC Adv.*, 2016, **6**, 89916 (ref. 96)
	Candle soot	Quenching	160–2000 nM	80 nM	*J. Lumin.*, 2016, **173**, 243 (ref. 97)
	Corn bract	Quenching	0–40 μM	9 nM	*Anal. Chem.*, 2017, **89**, 8044 (ref. 98)
	Citric acid, dimethylglyoxime	FRET	0.5–500 nM	0.1 nM	*Spectrochimica Acta, Part A*, 2021, **245**, 118924 (ref. 99)
	Glucose, dicyandiamide	Quenching		50 nM	*App. Surf. Sci.*, 2021, **544**, 148725 (ref. 100)
Ag	Carbon soot	Enhancement		500 pM	*Langmuir*, 2011, **27**, 4305 (ref. 101)
	Lactose	Quenching		385.8 nM	*J. Mater. Chem. A*, 2014, **2**, 8342 (ref. 102)
	N,*N*-Diisopropylcarbodiimide, *N*-hydroxysuccinimide	Quenching	12.3–61.9 mM	5.17 mM	*Anal. Chim. Acta*, 2015, **872**, 70 (ref. 103)
	Citric acid, ethylendiamine	Quenching	0.1–265 mM	50 nM	*Anal. Methods*, 2017, **9**, 5611 (ref. 104)
Mn	Diesel soot	Quenching	<10 mM		*J. Lumin.*, 2014, **146**, 37 (ref. 105)
Cr	Diethylenetriamine pentaacetic acid	Quenching	0.5–160 mM	0.15 mM	*J. Mater. Chem. B*, 2017, **5**, 2979 (ref. 106)
	Ammonium citrate	Quenching		0.01 μM	*Mater. Lett.*, 2017, **191**, 1–4 (ref. 107)
	$[PAVIm^+][Br^-]$	Quenching	0.05 and 10 μM	15 nM	*Talanta*, 2017, **165**, 216–222 (ref. 108)
	Benzoxazine	Quenching		0.58 mM	*RSC Adv.*, 2018, **8**, 7377 (ref. 109)
	o-Phenylenediamine	Enhancement	120 nM–200 mM	37 nM	*Microchem. J.*, 2021, **169**, 106552 (ref. 110)
Cu	Graphite rods	Quenching	0–50 mM	1 mM	*Angew. Chem., Int. Ed.*, 2012, **51**, 7185 (ref. 114)
	Grass	Quenching		1 nM	*Adv. Mater.*, 2012, **24**, 2037 (ref. 113)
	Lemon extract and L-arginine	Quenching	0.05–15 μM	0.047 μM	*Mater. Sci. Eng. C*, 2017, **75**, 1456 (ref. 115)
	Waste polyolefins	Quenching	1–8 μM	6.33 nM	*Sens. Actuators, B*, 2018, **254**, 197 (ref. 116)
	Sodium citrate, glutathione	Enhancement	< 1 mM	4.81 nM	*Analyst*, 2019, **144**, 4250 (ref. 117)
	Citric acid, ethylenediamine	Enhancement	0.025 to 4 μM	13 nM	*Anal. Bioanal. Chem.*, 2019, **411**, 2531 (ref. 118)
	Poly-thiophene carboxylic acid	Quenching	< 30 mM	0.44 mM	*Nano Res.*, 2019, **12**, 2576 (ref. 119)
	Human fingernails	Quenching	< 1 nM		*J. Environ. Chem. Eng.*, 2021, **9**, 104622 (ref. 120)
Fe	Dopamine	Quenching	< 20 mM	0.32 mM	*Chem.–Eur. J.*, 2013, **19**, 7243 (ref. 121)
	Alginate	Quenching	< 25 mM	1.06 mM	*Sens. Actuators, B*, 2015, **209**, 997 (ref. 122)
	Cyclic oligosaccharide	Quenching	16–166 mM	6.05 mM	*Spectrochim. Acta, Part A*, 2015, **150**, 934 (ref. 123)
	Citric acid, Tris	Quenching	< 50 mM	1.3 mM	*Talanta*, 2015, **143**, 107 (ref. 124)
	Trypsin, dopamine	Quenching	0.1 to 500 mM	30 nM	*Anal. Chim. Acta*, 2016, **926**, 107 (ref. 125)
	Dopamine, ethylenediamine	Quenching	50–300 mM	10.8 mM	*New J. Chem.*, 2016, **40**, 10213 (ref. 126)

Table 2 (*Contd.*)

Sensing	Carbon source	Mechanism of fluorescence detection	Linearity	LOD	Ref.
	Cranberry bean	Quenching	30–600 μM	9.55 μM	*ACS Omega*, 2019, **4**, 15382 (ref. 127)
	Poplar leaves	Quenching	0–2.5 μM	n.d.	*Chin. Chem. Lett.*, 2019, **30**, 2323 (ref. 128)
	Glucose, ethylenediamine	Quenching	< 50 μg mL^{-1}	3.3 ng mL^{-1}	*Food Chem.*, 2020, **308**, 125590 (ref. 129)
	Citric acid	Quenching	< 50 mM	0.172 mM	*Spectrochim. Acta, Part A*, 2020, **228**, 117717 (ref. 130)
Pb	Bovine serum albumin protein	Quenching	< 6 mM	5.05 mM	*Talanta*, 2013, **116**, 71 (ref. 131)
	Spinach extract	Quenching	< 500 mM	55 nM	*J. Mater. Chem. B*, 2019, **7**, 5502 (ref. 132)
	o-Phenylenediamine				*Sens. Actuators, B*, 2019, **288**, 749 (ref. 133)
	Orange peel	Quenching	0.5–1000 μM	0.25 μM	*Luminescence*, 2021, **6**, 1385 (ref. 134)
	PET bottle waste	Quenching	< 200 nM	21 nM	*New J. Chem.*, 2021, **45**, 8747 (ref. 135)
Al	Flaxseed oil	Quenching	< 35 mM	0.77 mM	*ACS Sustainable Chem. Eng.*, 2017, **5**, 3982 (ref. 136)
Au	MWCNTs	Quenching	0.65–4.37 nM	0.20 nM	*Anal. Chim. Acta*, 2014, **820**, 133 (ref. 137)
Halogen	Orange juice	Enhancement	1–20 μM	60 nM	*Langmuir*, 2015, **31**, 8111 (ref. 138)
	Citric acid, ethylenediamine	Quenching	< 140 μM	4 ppm	*Anal. Methods*, 2016, **8**, 1157 (ref. 139)

ions is essential to human health. However, the standard analytical methods, such as ICP-MS, require complex and high-cost protocols, and thus the possibility to use smart, sensitive and selective analytical methods is of practical interest.

Hg(II)

Due to the dangerous characteristics of mercury ions on human health, in particular the central nervous and endocrine system, the necessity to develop efficient detection methods to detect this metal ion in trace quantities is of primary importance. Sun and co-workers reported, for the first time, the sensing of Hg^{2+} by fluorescent CNPs obtained from candle soot.[90] In particular, these nanoparticles were modified with fluorescent-labeled DNA and its interaction with the nanoparticles quenched their emission. However, in the presence of Hg^{2+} ions, the DNA strand interacts with the metal ion, restoring the fluorescence (see Fig. 14). The selectivity was tested in the presence of several metal ion interferents, and good linearity was observed under 250 nM of mercury ions, and the limit of detection was 10 nM (Table 2).

Sun and co-workers developed three different nanosystems for the detection of mercury. In the first system, carbon nanoparticles (CNPs) synthesized *via* the hydrothermal treatment of pomelo peel were employed as a fluorescent probe for the label-free detection of Hg^{2+} ions.[91] The synthetic methodology developed has several advantages given that it allows fluorescent CNPs to be obtained, which are soluble in water with a quantum yield of about 6.9%, and it is simple and economical. Furthermore, the CNPs allowed the sensitive and selective detection of Hg^{2+}, given that in the presence of this ion, it is possible to observe a quenching of fluorescence, and the latter can only be restored in the presence of a stronger chelating agent for the Hg^{2+} ion, such as cysteine. This probe had a limit of detection for Hg^{2+} as low as 0.23 nM and was used for the detection of this ion in lake water samples.

Secondly, they synthesized carbon nanoparticles (CNPs) using a simple and green synthetic strategy, which involved microwave irradiation of an aqueous flour dispersion.[92] The CNPs exhibited properties such as water solubility and a quantum yield of about 5.4%, and in particular, could be used as fluorescent probes for the detection of Hg^{2+} ions. In fact, a linear range of 0.0005–0.01 μM and a detection limit of 0.5 nM were observed for the detection of these ions. Consequently, it was shown that the CNPs could be used for the detection of Hg^{2+} ions in real lake water samples.

In the third system, they developed a method for the green synthesis of CNPs, which involved the hydrothermal treatment of sweet potatoes.[93] In particular, the obtained CNPs were found to be soluble in water and have a quantum yield of approximately 2.8%. Furthermore, the CNPs could be used as a fluorescent probe for the label-free detection of Hg^{2+} ions. In fact, a detection limit for Hg^{2+} of 1 nM was observed, and therefore using this probe, it was possible to determine this ion in real water samples.

Zhang and co-workers synthesized a new type of nanohybrid system consisting of carbon nanoparticles (CNPs) and

Rhodamine B (RhB), assembled together *via* electrostatic attraction between the negative charge located on the CNPs and the positive charge located on the Rhodamine B dye, for the detection of Hg^{2+} ions (see Fig. 15).[94]

Upon irradiation at 350 nm, the CNP–RhB system showed two emission bands at 437 nm and 575 nm. In the presence of Hg^{2+} ions, the fluorescence of the CNPs was quenched, while unaltered fluorescence was observed for RhB. Also, the switching off of the fluorescence could also be observed with the naked eye under UV irradiation as a transition from violet to orange. For the detection of Hg^{2+} ions in different matrices (lake water and living cells), the CNPs–RhB nanohybrid system was sensitive and selective, with a detection limit of 42 nM. The low cytotoxicity of these nanoparticles allowed their application for intracellular measurements.

Ottoor and co-worker synthesized a new type of sensor for the detection of Hg^{2+} ions using carbon nanoparticles (CNPs) obtained *via* a green synthetic methodology and coconut milk as a precursor.[95] In particular, the obtained nanoparticles possessed different properties, which were soluble in water and in polar solvents, photostable and highly emissive. The quenching of the CNPs was studied using different metal ions that have a dangerous impact on ecological systems, and among them, the Hg^{2+} ion resulted in the significant quenching of the fluorescence of CNPs, with a detection limit of 16.5 nM and a linear response in the range of 30 to 50 nM.

Chen and co-workers synthesized nitrogen-doped CNPs using a facile one-pot and solid-phase approach, thus obtaining CNPs with a narrow size distribution and uniform surface state.[96] The doping helped to tune the intrinsic properties of the nanoparticles, expanding their fields of applications, such as bioimaging. In this study, the N-doped CNP probe was used to detect Hg^{2+} selectively and sensitively with an LOD of 2.3 nM and a linear range of 6–12 mM. The ion recognition is due to the coordination effect between the mercury ions and the pyrrolic-like N or N–H groups on the surface of the nanoparticles, leading quenching of the fluorescence. Sensing was successfully performed in complex matrices, such as food and cosmetics. Furthermore, the strong fluorescence of the CNPs was exploited to prepare a new type of fluorescent ink.

Paul and co-workers prepared CNPs from candle soot without the use of organic solvents.[97] These nanoparticles could detect two types of metal ions (Hg^{2+} and Fe^{3+}) in aqueous media in the presence of other metal ions as interferents. In fact, the interaction of the metal ions with the carboxyl groups on the nanoparticle surface led to the aggregation of the CNPs, and thus quenching of their emission was recorded, with an LOD of 80 nM for mercury ions and 40 nM for iron ions, and a linear range of 160–2000 nM (Fig. 16). Notably, these LOD values are lower with respect to other analytical methods reported in the literature.

Zhao and co-workers used the solvothermal approach to prepare, using corn bract as the starting material, nanohybrid CNPs with a dual-emission for the ratiometric sensing of Hg^{2+}.[98] This sensor, at a single excitation wavelength, showed two emission bands, namely, one at 470 nm and the other at 678 nm, having different behaviors in the presence of the analyte. In fact, the former was slightly modified, while the latter was strongly quenched in the presence of mercury ions. The ratiometric fluorescence response showed a linear response in the range of 0 to 40 μM of Hg^{2+} and a limit of detection of 9.0 nM.

Recently, Abdolmohammad-Zadeh and co-workers developed a sensor based on carbon and silver nanoparticles to detect Hg^{2+} *via* the FRET mechanism.[99] The starting fluorescence is quenched by FRET due to the interaction of the metal nanoparticles. The presence of mercury ion led to an increase in the emission due to the oxidation of the silver nanoparticles by the analyte. The authors reported a linear response in the range of 0.5–500 nM, with a limit of detection of 0.10 nM and a limit of quantification of 0.35 nM. Notably, this method was tested for the analysis of real samples, including lake water, wastewater and tea samples.

Similarly, Zhang and co-workers developed fluorescent N-doped CNPs *via* the thermal treatment of glucose and dicyandiamide (DCDA).[100] The presence of mercury ions resulted in the quenching of their emission at 441 nm, with a limit of detection of 50 nM.

Due to the dangerous nature of the Hg(II) ion, many efforts have been devoted to realizing efficient sensors. A brief overview

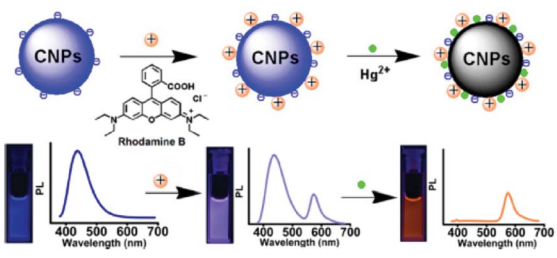

Fig. 15 Sensing mechanism of Hg^{2+} by CNPs containing RhB (reproduced with permission from *ACS Appl. Mater. Interfaces*, 2014, **6**, 21270–21278, Copyright 2014, the American Chemical Society).

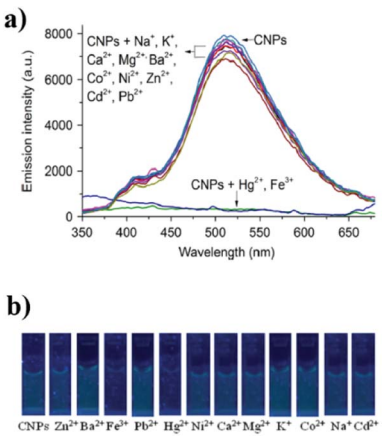

Fig. 16 (a) Emission spectra and (b) images of CNPs under a UV lamp in the presence of different cations upon excitation at 365 nm (reproduced with permission from *J. Lumin.*, 2016, **173**, 243–249, Copyright 2016, Elsevier).

of these systems highlights that green carbon sources are widely used for their synthesis, where the main fluorescence behavior is the quenching of the emission of CNPs due to the presence of mercury ions. In addition, the example reported in this review showed a wide concentration range for the detection of Hg^{2+} (from 0.5 nM to 6 mM), with the best LOD of 0.1 nM.

Ag(I)

The detection of silver ions has received much attention in recent years due to their widespread use in industry. The presence of excess of silver ions leads to some diseases, such as oxidative stress, exhaustion of organ function, growth retardation and mitochondrial damage. Thus, the detection of silver ions in drinking water is essential to prevent these problems. Sun and co-workers used CNPs as a fluorescent detection platform for the detection of Ag^+ ions by adopting the same approach employed for Hg^{2+} ion detection.[101] In fact, Ag^+ ions lead to the same behavior in the DNA strand, thus leading to an increase of the emission upon the progressive addition of Ag^+. The present sensing system showed a very low detection limit of 500 pM, with high selectivity for Ag^+ ions.

In the same context, Algarra and co-workers synthesized carbon dots from lactose in the presence of sulfuric acid.[102] Subsequently, the surface of the obtained nanoparticles was functionalized using mercaptosuccinic acid (MSA), obtaining CNP-MSA. The presence of these groups on the surface of carbon dots makes them useful as fluorescent sensors for the detection of Ag^+ ions. In fact, in the presence of Ag^+ ions, fluorescence quenching of CNP-MSA was observed, and this probe was selective and sensitive, showing a limit of detection and quantification of 385.8 nM and 1.2 μM, respectively.

Valcárcel and co-workers synthesized a fluorescent sensor for the detection of citrate–silver nanoparticles (cit-AgNPs) using CNPs functionalized with amino groups.[103] Also, in this case, the sensing of cit-AgNPs led to the quenching of the emission of the CNPs. This sensor was reusable but required the presence of EDTA to remove other metal ions as interferences. Furthermore, a linear correlation was observed in the range of 1.23×10^{-5} to 6.19×10^{-5} M, with a limit of detection and quantification of 5.17×10^{-6} M and 1.72×10^{-5} M, respectively.

Subsequently, Wang and co-workers synthesized water-soluble CNPs *via* the hydrothermal method.[104] These nanoparticles, showed an emission peak at 441 nm upon excitation at 352 nm. The CNPs reduced Ag(I) to Ag(0), thus leading to the formation of silver aggregates on their surface. Then, cysteine molecules could be adsorbed on the above-mentioned hybrid carbon nanoparticles through the formation of Ag–S bonds, inducing aggregation and forming a CNP/Cys assembled system that could monitor the concentration of the analyte in two different ways (Fig. 17). Specifically, observing the quenching of the fluorescence intensity, which is directly proportional to the concentration of the ions in the range of 0.1 mM to 265 mM with an LOD of 50 nM, and observing the light-scattering intensity, showing an enhancement proportional to the concentration of Ag^+ from 10 to 4000 nM with a detection limit of about 2 nM.

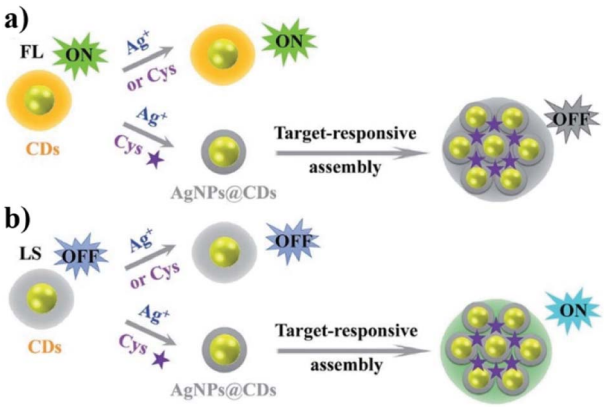

Fig. 17 Representation of CNPs for Ag^+ sensing *via* (a) fluorometric and (b) light-scattering (reproduced with permission from *Anal. Methods*, 2017, **9**, 5611–5617, Copyright 2017, The Royal Society of Chemistry).

Furthermore, this sensor was studied using real water samples, also showing a good selective response in the presence of different types of metal ions.

In the case of silver ions, less examples compared to mercury have been reported. Also in this case, quenching of the emission is the main mechanism of detection. The concentration range used for the detection of silver and the limits of detection are higher with respect to mercury (millimolar). However, with an enhancement in the emission in the presence of Ag(I) ions, the limit of detection decreased dramatically to 500 pM.

Mn(II)

Exposure to manganese ions in air at concentrations more than 5 μg m^{-3} can lead to manganism, a biphasic disorder mainly linked to impaired motor skills, cognitive disorders, compulsive behaviors, and psychosis, which resembles Parkinson's disease. Wang and co-workers synthesized another type of fluorescent carbon nanoparticles (CNPs) *via* the nitric acid oxidation of diesel soot.[105] Using this synthetic method, a wide size distribution of carbon nanoparticles was obtained and dimensional separation was adopted to separate the smallest particles (ULCNPs) from the biggest particles (LLCNPs). The color of the ULCNP solution underwent an alteration as the pH of the solution varied, which was not observed for LLCNPs, and this could be beneficial for some applications such as the detection of the acidity or alkalinity of a solution. In addition, studies on the use of these carbon nanoparticles as sensors capable of detecting metal ions were conducted. In particular, the fluorescence intensity of the ULCNPs was slightly quenched by Mn^{2+} ions and not by other metal ions, with a linear response up to 10 mM. However, the fluorescence intensity of the LLCNPs remained unchanged in the presence of all metal ions.

Cr(VI)

The Cr(VI) ion represents one of the most toxic heavy metal ions, and thus its use has been drastically reduced in the last few years. Its concentration in drinking water is strictly controlled

and must be lower than the micromolar level. Due to the carcinogenicity and genotoxicity of this metal ion, the World Health Organization fixed it at a risk level of 50 μg L^{-1}.

A Cr(VI) nanosensor was proposed by Li and co-workers, which was synthesized *via* the calcination of diethylenetriaminepentaacetic acid (DTPA), thus obtaining water-soluble nitrogen-doped nanoparticles (N-CNPs).[106] These CNPs could be used to quickly determine Cr^{6+} ions through turn-off of fluorescence due to the inner filter effect (IFE) process. This sensing showed linearity in the range of 0.5–160 mM, with a calculated detection limit of 0.15 mM. It was also possible to recover the fluorescence intensity and inhibit the IFE process using ascorbic acid, which led to the reduction of Cr^{6+} to Cr^{3+}. Thus, the authors proposed the use of this system not only to detect chromium ions in water samples, but also for the determination of ascorbic acid in human serum samples.

Zheng and co-workers synthesized, using a one-step hydrothermal approach, carbon nanoparticles from ammonium citrate.[107] These CNPs were used to detect Cr(VI) ions and sulfites through the fluorescence quenching caused by the electron exchange interaction between the nanoparticle surface and the metal ion. Then, the fluorescence could be recovered by the reduction of chromium(VI) to Cr(III) by the sulfite anion. This nanosensor showed a detection limit of 0.01 mM for chromium and 0.35 mM for sulfites, demonstrating good sensitivity.

Zhang and co-workers reported the synthesis of CNPs using a green protocol *via* the microwave pyrolysis of an ionic liquid (1-vinyl-3-aminopropyl imidazolium, [$PAVIm^+$][Br^-]) as the carbon source and ethylenediamine, which allowed N-doping.[108] The obtained nanoparticles exhibited the capability to detect Cr(VI) ions following the quenching of their fluorescence. A linear response was detected between 0.05 and 10 mM, with a limit of detection of 0.015 mM. The optimum photoluminescence properties were used not only for the determination of chromium ions in real samples but also for the determination of the temperature and the pH value. In fact, there are many carboxyl and amino groups on the surface of the CNPs, which can be protonated and deprotonated, thus obtaining a system sensible with a variation in pH, and furthermore, the system also showed a gradual decrease in luminescence with an increase in the temperature in a linear range.

Cao and co-workers reported the use of benzoxazine (BZ) as the starting material to obtain basophilic green fluorescent carbon nanoparticles (G-CNPs) *via* a hydrothermal procedure.[109] The obtained G-CNPs showed good water solubility in alkaline pH due to the presence of free carboxylic acids on their surface. The authors proposed the use of these nanoparticles to detect Cr(VI) in extreme alkaline conditions. In particular, this ion leads to a strong quenching of the emission due to its internal filter effect (IFE). In addition, they obtained a selective and fast response to Cr(VI), with a limit of detection of 0.58 μM.

Recently, Ma and co-workers developed a simple and sensitive ratiometric sensor based on the coordination between Cr(VI) and CNPs, which were prepared using *o*-phenylenediamine (oPD) as a precursor.[110] These nanoparticles showed an emission in the blue region upon excitation at 388 nm, which after interaction with Cr^{6+} changed to orange. In fact, in the presence of Cr(VI), the initial emission at 445 nm shifted to 565 nm, with an increase in intensity. This sensor showed a linear response to Cr(VI) in the range of 120 nM to 200 mM, with an LOD of 37 nM. Notably, this system was used for the analysis of real water samples.

Curiously, carbon nanoparticles for the detection of Cr(VI) are not synthesized starting from "green carbon atoms". Quenching of the emission is the main detection mechanism, and the concentration ranges used are generally high (from micro to millimolar).

Cu(II)

The copper ion is one of the most abundant metal ions in biological systems. It is involved in many fundamental intracellular processes and its misregulation seems to be related to important neurodegenerative diseases. Thus, the possibility to monitor the intracellular level of copper using fluorescent probes is fundamental to understand the initial steps in these disorders.[111,112]

Sun and co-workers employed a green and cost-effective synthetic strategy to obtain a fluorescent detection platform for the label-free detection of Cu^{2+} ions, namely photoluminescent polymer nanodots (PPNDs).[113] These PPNDs were synthesized *via* the hydrothermal treatment of grass and exhibited interesting properties such as water solubility and photoluminescence. Furthermore, depending on the temperature at which the reaction was carried out, it was possible to vary the dimensions and the quantum yield of the PPNDs, where the quantum yield increased as the temperature increased and the dimensions decreased as the temperature increased. The detection of Cu^{2+} ions appeared to be possible in a sensitive and selective way and an LOD as low as 1 nM was observed; therefore, PPNDs were used to detect Cu^{2+} ions in real water samples.

Tian and co-workers designed a hybrid ratiometric probe based on fluorescent CNPs with a specific receptor for Cu^{2+} ions, *i.e.*, *N*-(2-aminoethyl)-*N*,*N*,*N*′-tris(pyridin-2-ylmethyl) ethane-1,2-diamine (AE-TPEA).[114] In particular, the hybrid system, composed of CdSe and ZnS, mixed with carbon nanoparticles showed two emission bands at 485 nm and 644 nm, using a single excitation wavelength. The functionalization of the CNPs with AE-TPEA led to blue fluorescence (485 nm), while the CdSe/ZnS CNPs showed red fluorescence (644 nm). In the presence of Cu^{2+} ions, the receptor site recognized these ions, and thus quenching of the blue fluorescence was observed, while the red fluorescence of the CdSe/ZnS CNPs remained unaltered. A linear response was observed under 50 mM and the calculated limit of detection was 1 mM, with good selectivity in the presence of other metal ions and amino acids.

Later, Das and co-workers prepared N-doped CNPs using lemon extract and L-arginine as starting materials for the detection of Cu^{2+} in aqueous medium.[115] This ion interacts with the amino groups on the surface of the CNPs, forming a cupric ammine complex, which resulted in the quenching of the fluorescence *via* the inner filter effect. This system showed good

sensitivity for Cu^{2+} in a wide concentration range (0.05–300 μM), with good linearity under 15 mM and an LOD of 0.047 μM.

Kumari and co-workers proposed that the residue obtained from the pyrolysis of waste polyolefins could be used for the synthesis of green-fluorescent carbon quantum dots, having good stability, high selectivity, sensitivity and fast response for sensing Cu^{2+} ions.[116] The authors reported that different Cu^{2+} concentrations led, after five minutes, to a color change in the CNPs solution. These nanoparticles showed a linear response to Cu^{2+} in the range of 1–8 μM, with a detection limit of 6.33 nM. Due to the low toxicity, good cell permeability, and good fluorescence properties of the CNPs, the authors also performed cellular imaging, suggesting their potential application in the treatment of the breast cancer.

Wei and co-workers reported a new nanosensor for the detection of Cu^{2+} ions in aqueous solution, with high selectivity and sensitivity compared to other metal ions.[117] In particular, this system exploited the emission and color change to monitor copper. This sensor consisted of hybridized carbon and gold–silver nanoparticles (Au@AgNPs). The fluorescence of the CNPs was quenched by Au@AgNPs and recovered by Cu^{2+} in the presence of thiosulfate. The colorimetric changes were due to the SPR shift of Au@AgNPS in the presence of copper. This dual probe showed excellent selectivity and a linear response under 1 μM of Cu^{2+}, with a limit of detection of 4.81 nM for emission measurements and 3.85 nM for colorimetric measurements.

Ren and co-workers reported the synthesis of a ratiometric fluorescent sensor for Cu^{2+} from blue-emitting N-doped CNPs in silica, covalently functionalized with terminal amino groups, which interact with the carboxylic groups of modified gold nanoclusters (AuNCs).[118] In the presence of copper ions, the emission of the AuNCs was quenched, but the fluorescence of the CNPs remained unaltered due to the shielding effect of silica. This sensor could detect Cu^{2+} in the range of 0.025 to 4 μM, with a detection limit of 0.013 μM, in real mineral water samples.

Zhang and co-workers prepared CNPs with an emission wavelength ranging from 483 to 525 nm, having different degrees of surface oxidation and different sizes depending on the concentration on NaOH during the synthetic process.[119] The emission properties, in terms of wavelength, could be modulated by the amount of NaOH, where in particular, with an increase in the amount of base, the emission wavelength increased. These CNPs could be used as ratiometric fluorescence sensors for the detection of copper with a fast, selective and sensitive response and applied for the analysis of pond water and living cells. This is due to the functional groups present on their surface (–OH, –COOH and SO_4^{2-}), which allow them to coordinate Cu^{2+} ions, leading to quenching of their emission. This system showed good linearity under 30 mM and a detection limit of 0.44 μM.

Recently, Sim and co-workers reported the use of CNPs obtained *via* the hydrothermal treatment of human fingernails as a green precursor for the sensing of copper ions.[120] These nanoparticles, also used for the photodegradation of 2,4-dichlorophenol (2,4-DCP) under sunlight, could selectively detect copper ions at a concentration as low as 1 nM, following the quenching of their emission.

In summary, copper detection can be performed in general *via* quenching of the emission, in a concentration range of micro to millimolar. Notably, the limits of detection can be found in the nanomolar levels, thus leading to their potential application for the biological determination of copper.

Fe(III)

The Fe^{3+} ion is one of the most widespread metal ions in the human body and also in the environment. However, its excess causes many problems, such as liver damage, kidney failure, and even death. Qu and co-workers designed a fluorescent sensor using carbon nanoparticles (CNPs) obtained using dopamine as a precursor.[121] The sensing mechanism is due to the ability of the catechol units on the carbon nanoparticle surface to be oxidized by Fe^{3+} ions, thus leading to strong quenching of its emission. The presence of free dopamine in solution could restore the starting emission due to the competition with the redox reaction (Fig. 18). A detection limit of 0.32 μM and 68 nM was observed for the detection of Fe^{3+} ions and dopamine, respectively. Also, selectivity in the presence of other metal ions and organic molecules was demonstrated.

Ng and coworkers synthesized a fluorescent sensor based on CNPs, which were obtained starting from alginate and using a simple two-step synthesis procedure.[122] The obtained CNPs obtained had small dimensions and high photoluminescence. Furthermore, this fluorescent sensor could be used for the sensitive and selective detection of ferric ions. In fact, the presence of hydroxyl and carboxyl groups on the surface of the CNPs allowed their interaction with the Fe^{3+} ions, and consequently fluorescence quenching. A linear dynamic range up to 25 μM and a limit of detection of 1.06 μM were observed.

Finally, it was shown that the developed sensor could be used for the detection of Fe^{3+} ions in a real water sample.

Rasoulzadeh and co-workers designed a CNP sensor, starting from the cyclic oligosaccharide α-CD, for the sensitive and selective detection of ferric ions due to the fluorescence quenching of the CNPs in the presence of these ions.[123] In aqueous solution, the detection of Fe^{3+} ions was carried out also in the presence of interfering metal ions, demonstrating the high selectivity. A linear relationship was observed in the range of 16–166 mM and a detection limit of 6.05 mM.

Zhou and co-workers synthesized a fluorescent sensor for Fe^{3+} based on carbon nanoparticles using an easy and green synthesis, which involved the use of citric acid and Tris as

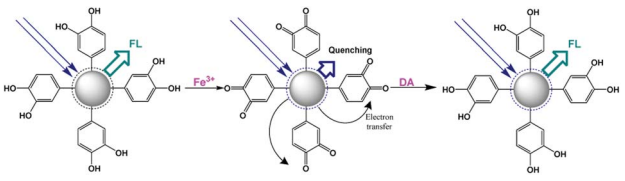

Fig. 18 Sensing mechanism for Fe^{3+} and dopamine by CNPs functionalized with catechol.

precursors.[124] The CNPs exhibited strong blue photoluminescence as function of pH. The detection of ferric ions led to a fluorescence quenching, with a good linear correlation below 50 μM and a limit of detection of 1.3 μM. Finally, it was shown that the CNPs could be used for the detection of Fe^{3+} ions in tap and lake water but the use of this sensor could be extended to other fields of application, such as biological imaging, due to its low toxicity and biocompatibility.

Chen and co-workers synthesized blue-green fluorescent CNPs using trypsin and dopamine as starting materials.[125] These CNPs were used as a "turn-off" fluorescence sensor due to the inner filter effect and static quenching mechanism to detect Fe^{3+} ions sensitively and selectively, showing a linear range from 0.1 to 500 mM, with a limit of detection of 30 nM. The authors also demonstrated high selectivity in the presence of competing ions. Furthermore, the sensor could also be used to detect iron ions in biological samples, such as urine and serum.

Zhang and co-workers reported the preparation of nitrogen-doped CNPs *via* hydrothermal treatment, with dopamine and ethylenediamine as starting materials, to detect Fe^{3+} under acidic conditions.[126] These N-CNPs showed an emission band at 497 nm and high stability at low pH values. The interaction between the nanoparticles and iron ions can be explained by highlighting that the functional groups on their surface, which are primary amines and catechol groups, can be oxidized to quinone species by Fe^{3+}, causing a variation in fluorescence (Fig. 19). This study demonstrated the possibility to determine these ions in acidic conditions, in the linear range of 50–300 mM with a detection limit of 10.8 mM.

Huang and co-workers described the synthesis of fluorescent CNPs derived from cranberry bean (CB) *via* hydrothermal treatment.[127] This sensor showed stable fluorescence with a quantum yield of about 10.85%, giving a strong bright blue fluorescence color under UV light irradiation. This sensor was used for the detection of Fe^{3+} ions by excitation at 380 nm in a wide metal concentration range (30–600 μM), with a detection limit of 9.55 μM. In particular, Fe^{3+} ions led to strong quenching of the fluorescence intensity of the carbon nanoparticles, thus leading to high selectivity (Fig. 20).

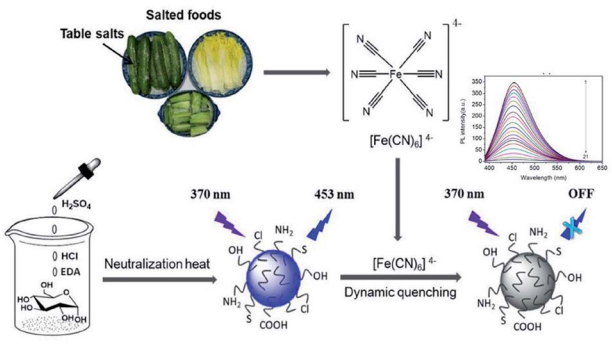

Fig. 19 Schematic representation of fluorescence enhancement and the Fe^{3+} detection process of the N-CD probe (reproduced with permission of *New J. Chem.*, 2016, **40**, 10213–10218, Copyright 2016, The Royal Society of Chemistry).

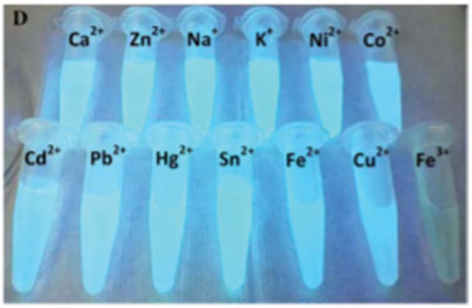

Fig. 20 Image of CNPs derived from cranberry bean in the presence of different cations under Vis excitation (reproduced with permission from *ACS Omega*, 2019, **4**, 15382–15392, Copyright 2019, the American Chemical Society).

Yang and co-workers proposed a synthetic strategy to obtain CNPs *via* a simple, economical, green and useful large-scale process.[128] In particular, by treating poplar leaves using a one-step hydrothermal method, it was possible to obtain more than one kilogram of CNPs. Moreover, thanks to some properties such as stability in aqueous solvents, photoluminescence and low cytotoxicity, some applications of the CNPs studied in this work included the selective detection of Fe^{3+} ions in water samples and use as a biological probe for bioimaging.

Recently, Yang and co-workers reported the preparation of fluorescent nanoparticles doped with nitrogen, sulphur and chlorine (N,S,Cl-CNPs), for the sensing of ferrocyanide ions $[Fe(CN)_6]^{4-}$ in the food matrix.[129] The starting materials used for this sensor were glucose, hydrochloric acid, sulphuric acid and ethylenediamine (Fig. 21). The sensing mechanism is due to the quenching effect of the $[Fe(CN)_6]^{4-}$ ion on the emission of the nanoparticles. This sensor showed high selectivity with respect to other ionic species, a linear response under 50 μg mL^{-1}, LOD of 3.3 ng mL^{-1} and LOQ of 11 ng mL^{-1}.

Nan and co-workers reported the use of a hybrid nanosensor for the detection of Fe^{3+} based on a simple and fast spectrofluorimetric analysis.[130] They fabricated this sensor using ZnO/CdS nanoparticles modified with carbon nanoparticles. The sensing is based on the strong fluorescence quenching of the nanoparticles by the Fe^{3+} ion due to the strong interaction between them and iron ions. The calculated LOD of this system was 0.172 mM, with a linear response below 50 mM and good selectivity.

In summary, iron sensing by CNPs can be monitored, in all cases, by a quenching of their fluorescence emission. Different

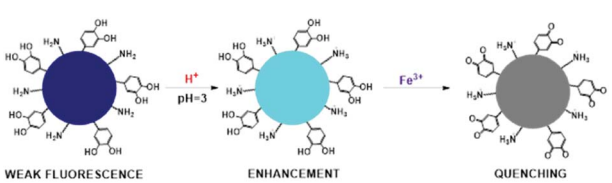

Fig. 21 Synthesis of N,S,Cl-CNPs and schematic representation of the $[Fe(CN)_6]^{4-}$ sensing (reproduced with permission from *Food Chem.*, 2020, **308**, 125590, Copyright 2020, Elsevier).

carbon sources can be used for the synthesis of these nanoparticles (natural or synthetic), obtaining sensors that can detect iron at millimolar (in most of the cases) or micromolar concentrations. Notably, the limit of detection is at the nanomolar level in a few cases.

Pb(II)

The Pb(II) ion represents one of most dangerous water pollutants due to its negative effects on bones, the liver, kidney, brain, and cardiovascular and central nervous systems. The World Health Organization recommended a limit of 10 μg L^{-1} in drinking water. Muk Ng and co-workers proposed an economical and green method for the synthesis of carbon nanoparticles from bovine serum albumin protein.[131] The carbon nanoparticles obtained showed high fluorescence and stability under different pH values, and the selective detection of Pb^{2+} ions led to a significant decrease in fluorescence emission, with a limit of detection of 5.05 μM.

Dong and co-workers reported the use of ratiometric fluorescent nanoparticles for the sensing of Pb^{2+} exploiting a dual emission band (477 and 651 nm), under single wavelength excitation (391 nm).[132] This sensor showed high selectivity and sensitivity toward Pb^{2+} compared to other analytes, with a detection limit of 0.055 mM and a linear ratiometric response under 500 mM. Notably, the sensing of Pb ions could be observed also with the naked eyes by following the color change from pink to cyan (Fig. 22).

Yu and co-workers reported the synthesis of CNPs *via* chemical oxidative polymerization, using *o*-phenylenediamine (o-PD) and ammonium persulfate (APS) as the starting materials.[133] The presence of many diamine groups on the surface of the CNPs led to the possibility of them interacting with many metal ions, thus leading to a change in absorbance and emission properties. This system was used to detect eight metal ions, including Cr^{3+}, Cu^{2+}, Fe^{3+}, Hg^{2+}, Cd^{2+}, Pb^{2+}, Co^{2+}, and Ni^{2+}, in the micromolar concentration range, which were differentiated by principal component analysis (PCA). This method was applied and validated for the identification of 48 unknown samples and spiked lake water.

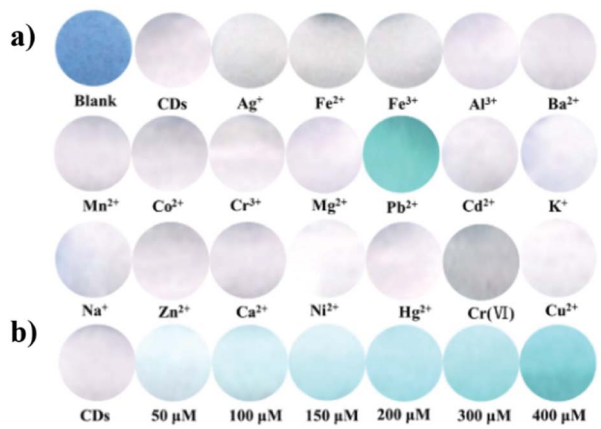

Fig. 22 Photos of strips containing CNPs and (a) different metal ions and (b) with different amounts of Pb^{2+} (reproduced with permission from *J. Mater. Chem. B*, 2019, **7**, 5502, Copyright 2019, The Royal Society of Chemistry).

Recently, Hu and co-workers reported the use of CNPs synthesized from orange peel as a precursor to detect Fe^{3+} ions.[134] The authors demonstrated how the presence of ethanol improved the sensing properties, with a detection limit of 0.25 μM and a linear response in the range of 0.5–1000 μM. The selectivity tests demonstrated good selectivity for Fe^{3+} ions. In addition, this sensor was used for the analysis of real tap water samples.

Recently, Das and co-worker synthesized green fluorescent CNPs using PET bottle waste as a carbon source to sustainably recycle and safely dispose of polyethylene terephthalate waste.[135] The obtained CNPs showed interesting optical properties and selectivity for lead ions through a strong fluorescence quenching effect. A linear response was observed under 200 nM, with a calculated LOD of 21 nM. The authors highlighted that this linear range is the lowest with respect to other recent analytical methods based on carbon nanoparticles.

Nanoparticles for the detection of lead can be obtained using natural or polymeric sources. As observed for the detection of iron, quenching of the emission is the mechanism of sensing. The concentration levels used are wide (from nanomolar to millimolar), as well as the limits of detection.

Al(III)

Kim and co-workers synthesized water-soluble oxidated onion-like-CNPs *via* the pyrolysis of flaxseed oil.[136] These CNPs showed green emission and were used to degrade methylene blue (MB) under visible light irradiation. The water-soluble CNPs exhibited enhanced photocatalytic efficiency, which can be attributed to the functionalities on their surface and their nanostructure. The catalytic activity was enhanced by the high absorption of MB on the nanoparticle surface. Furthermore, these nanoparticles demonstrated capability for the specific detection of Al(III) ions through the fluorescence turn-off effect, even in the presence of high concentrations of other metal ions, with a linear response below 35 mM and a detection limit of 0.77 μM.

Au

Aluminium is the third most abundant heavy metal ion in the Earth's surface and can be found in water due to industrial activity, water treatment, and the pharmaceutical and cosmetic industries. Increased levels of Al can be related to important diseases, such as Alzheimer's disease, Parkinson's disease, and breast cancer. Valcárcel and co-workers synthesized CNPs functionalized with thiol terminal groups on the surface for the development of a fluorescent sensor for the detection of gold nanoparticles (AuNPs).[137] In fact, in the presence of gold nanoparticles, the thiol groups on the CNP surface allow the formation of the CNP–AuNP system, with consequent quenching of the carbon nanoparticle fluorescence by the static quenching mechanism. Notably, this method was tested on environmental (drinking water) and biological matrices (mussel tissues), with a limit of detection and quantification of 0.20 and 0.66 nM, respectively. Furthermore, the method for the detection of AuNPs is particularly satisfactory when EDTA is present in the matrix,

given that it allows selective interaction with the AuNPs in the presence of interferents (metallic species).

Halogens

Free chlorine represents the main ingredient of disinfectants in urban tap water and is widely used in medicine and for water treatment. It can be internalized by inhalation, diet and skin contact. Excess free chlorine is related to palm sweating and hair loss. The recent scenario has resulted in a strong increase in the use of disinfectants, resulting in an increase in chlorine levels.

Mohapatra and co-workers developed a sensor capable of detecting and removing fluoride ions from aqueous solutions.[138] The detection could be performed using the sensor consisting of a receptor–fluorophore system and the removal of the sensor could be performed using an external magnetic field, where a special feature of this sensor is that it can be reused. In particular, this system consisted of a magnetic receptor, such as magnetite nanoparticles coated with silica functionalized with a nickel-ethylenediaminetetraacetic acid complex (Fe_3O_4@SiO_2–EDTA–Ni), and a fluorophore such as highly fluorescent CNPs. The covalent bond between the magnetic receptor and the fluorophore led to partial fluorescence quenching of the CNPs. In the presence of F^- ions, gradual restoration of the fluorescence of the CNPs was observed due to the exchange of the carbon nanoparticles with the F^- ions on the magnetic receptor. A limit of detection of 0.06 μM and a linear range of 1 to 20 μM were observed. The aforementioned sensor was used for the detection of F^- ions in tap water, and due to its biocompatibility, it could be used for the detection and imaging of these ions in living cells.

Yan and co-workers reported a hybrid nanosystem in which CNPs were mixed with rhodamine B (RhB) for the realization of a fluorescent sensor to quantitatively detect free chlorine in water.[139] The presence of NaClO led to a charge transfer interaction, thus leading to quenching of the emission at 445 nm, while the emission of RhB (580 nm) remained unaltered. This ratiometric behavior led to a change in color, allowing the possibility to detect NaClO with the naked eyes at a concentration below 140 mM (Fig. 23), with a limit of detection of 4 ppm.

Conclusions and future perspectives

Carbon nanoparticles represent a relatively new class of organic nanostructures, which during the last few years, represent a new frontier not only for chemists. In fact, these nanomaterials have been applied in many fields, including sensing. This review summarized the application of fluorescent carbon nanoparticles in chemical and ion sensing, focusing on useful analytical parameters, such as their linear range of response and limit of detection. Some interesting points can be highlighted, as follows:

(a) From an optical point of view, a clear difference between chemical and ion sensing can be represented by the mechanism of fluorescence detection. In general, chemical sensing of single molecules can be monitored by following quenching or enhancement of the emission of CNPs, depending on the guest. Furthermore, in general, sensing *via turn-on* of the emission in the presence of the analyte (due to the PET and FRET mechanism) leads to lower limit of detection values, thus obtaining more sensitive sensors. On the contrary, ion sensing is occurs *via* quenching of the emission due to the interaction of the metal ion with the nanoparticle. In general, a turn-on sensor in which an enhancement in emission can be recorded after exposure to the analyte is preferred with respect to a turn-off sensor. Thus, a possible improvement in this field can be the design of new fluorescent carbon nanoparticles that undergo an increase in emission after the addition of specific ions.

(b) Few examples cover a wide concentration range with a linear fluorescence response. In general, the linearity of these probes covers a short range. Thus, an additional future target should be the improvement of the linearity range, thus obtaining nanosensors that are suitable for a wide concentration of guest molecules.

(c) Particularly, from our point of view, synthetic procedures to obtain carbon nanoparticles starting from waste materials (food grade honey, silkworm droppings, candle soot, corn bract, carbon and diesel soot, lemon extract, waste polyolefins, human fingernails, cranberry bean, orange peel, PET bottle waste, and orange juice) are interesting. This approach can lead to an improvement in recovery processes, in particular in the agro-food industry, to obtain new starting materials for organic chemists.

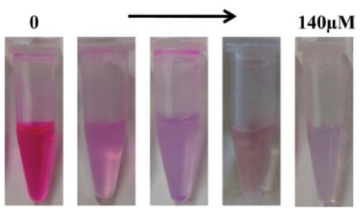

Fig. 23 Images of CNP solution for NaClO sensing upon the addition of different concentrations of NaClO (reproduced with permission from *Anal. Methods*, 2016, **8**, 1157–1161, Copyright 2016, The Royal Society of Chemistry).

Conflicts of interest

There are no conflicts to declare.

Acknowledgements

The authors acknowledge the University of Catania for the funding received under the starting grant "DetCWAs" (PIA.-CE.RI 2020-2022-Linea Intervento 3), PIA.CE.RI. 2020-2022 Linea 1 Chance and the project MAFmoF "Materiali multifunzionali per dispositivi micro-optofluidici".

Notes and references

1 V. Vakhrushev, V. I. Kodolov, A. K. Haghi and S. C. Ameta, *Carbon Nanotubes and Nanoparticles: Current and Potential Applications*, CRC Press, Taylor & Francis Group, 1st edn, 2019.
2 C. Testa, A. Zammataro, A. Pappalardo and G. Trusso Sfrazzetto, *RSC Adv.*, 2019, **9**, 27659–27664.

3 Y. Wang, Y. Zhu, S. Yu and C. Jiang, *RSC Adv.*, 2017, **7**, 40973–40989.
4 X. T. Zheng, A. Ananthanarayanan, K. Q. Luo and P. Chen, *Small*, 2015, **11**, 1620–1636.
5 A. Zammataro, C. M. A. Gangemi, A. Pappalardo, R. M. Toscano, R. Puglisi, G. Nicotra, M. E. Fragalà, N. Tuccitto and G. Trusso Sfrazzetto, *Chem. Commun.*, 2019, **55**, 5255–5258.
6 Y. An, X. Lin, Y. Zhou, Y. Li, Y. Zheng, C. Wu, K. Xu, X. Chai and C. Liu, *RSC Adv.*, 2021, **11**, 26915–26919.
7 W. Su, H. Wu, H. Xu, Y. Zhang, Y. Li, X. Li and L. Fan, *Mater. Chem. Front.*, 2020, **4**, 821–836.
8 A. M. El-Shafey, *Green Process. Synth.*, 2021, **10**, 134–156.
9 W. Wang, C. Damm, J. Walter, T. J. Nacken and W. Peukert, *Phys. Chem. Chem. Phys.*, 2016, **18**, 466–475.
10 P. Mate, A. Chandimeshram, K. Wadher and M. Umekar, *World J. Pharm. Res.*, 2020, **9**, 971–979.
11 S. Dugam, S. Nangare, P. Patil and N. Jadhav, *Ann. Pharm. Fr.*, 2021, **79**, 335–345.
12 N. Mauro, M. A. Utzeri, P. Varvara and G. Cavallaro, *Molecules*, 2021, **26**, 3085.
13 B. D. Mansuriya and Z. Altintas, *Nanomaterials*, 2021, **11**, 2525.
14 S. Šafranko, D. Goman, A. Stankovic, M. Medvidovic-Kosanovic, T. Moslavac, I. Jerkovic and S. Jokic, *Chemosensors*, 2021, **9**, 138.
15 M. J. Molaei, *RSC Adv.*, 2019, **9**, 6460–6481.
16 X. Xu, R. Ray, Y. Gu, H. J. Ploehn, L. Gearheart, K. Raker and W. A. Scrivens, *J. Am. Chem. Soc.*, 2004, **126**(40), 12736–12737.
17 Y.-P. Sun, B. Zhou, Y. Lin, W. Wang, K. A. S. Fernando, P. Pathak, M. J. Meziani, B. A. Harruff, X. Wang, H. Wang, P. G. Luo, H. Yang, M. E. Kose, B. Chen, L. M. Veca and S.-Y. Xie, *J. Am. Chem. Soc.*, 2006, **128**(24), 7756–7757.
18 S. Zhu, Q. Meng, L. Wang, J. Zhang, Y. Song, H. Jin, K. Zhang, P. H. Sun, H. Wang and B. Yang, *Angew. Chem., Int. Ed.*, 2013, **52**, 3953–3957.
19 Y. Hou, Q. Lu, J. Deng, H. Li and Y. Zhang, *Anal. Chim. Acta*, 2015, **866**, 69–74.
20 S.-L. Hu, K.-Y. Niu, J. Sun, J. Yang, N.-Q. Zhao and X.-W. Du, *J. Mater. Chem.*, 2009, **19**, 484–488.
21 N. Tuccitto, G. Li-Destri, G. M. L. Messina and G. Marletta, *J. Phys. Chem. Lett.*, 2017, **8**(16), 3861–3866.
22 J. Liu, D. Li, K. Zhang, M. Yang, H. Sun and B. Yang, *Small*, 2018, **14**, 1703919.
23 H. Zhu, X. Wang, Y. Li, Z. Wang, F. Yang and X. Yang, *Chem. Commun.*, 2009, 5118–5120.
24 R. Ludmerczki, S. Mura, C. M. Carbonaro, I. M. Mandity, M. Carraro, N. Senes, S. Garroni, G. Granozzi, L. Calvillo, S. Marras, L. Malfatti and P. Innocenzi, *Chem.–Eur. J.*, 2019, **25**, 11963–11974.
25 Z.-C. Yang, M. Wang, A. M. Yong, S. Y. Wong, X.-H. Zhang, H. Tan, A. Y. Chang, X. Li and J. Wang, *Chem. Commun.*, 2011, **47**, 11615–11617.
26 S. Tao, S. Zhu, T. Feng, C. Xia, Y. Song and B. Yang, *Mater. Today Chem.*, 2017, **6**, 13–25.
27 Y. Yang, J. Cui, M. Zheng, C. Hu, S. Tan, Y. Xiao, Q. Yang and Y. Liu, *Chem. Commun.*, 2012, **48**, 380–382.
28 F. Calì, V. Cantaro, L. Fichera, R. Ruffino, G. Trusso Sfrazzetto, G. Li-Destri and N. Tuccitto, *Chemosensors*, 2021, **9**, 202.
29 K. Jiang, S. Sun, L. Zhang, Y. Lu, A. Wu, C. Cai and H. Lin, *Angew. Chem., Int. Ed.*, 2015, **54**, 5360–5363.
30 H. Lin, J. Huang and L. Ding, *J. Nanomat.*, 2019, 5037243.
31 D. Qu, X. Wang, Y. Bao and Z. Sun, *J. Phys. Mater.*, 2020, **3**, 022003.
32 P. Koutsogiannis, E. Thomou, H. Stamatis, D. Gournis and P. Rudolf, *Adv. Phys.: X*, 2020, **5**, 1758592.
33 P. Anilkumar, X. Wang, L. Cao, S. Sahu, J.-H. Liu, P. Wang, K. Korch, K. N. Tackett II, A. Parenzan and Y.-P. Sun, *Nanoscale*, 2011, **3**, 2023–2027.
34 N. Dhenadhayalan, K.-C. Lin, R. Suresh and P. Ramamurthy, *J. Phys. Chem. C*, 2016, **120**, 1252–1261.
35 A. Prasanna de Silva, T. S. Moodyband and G. D. Wright, *Analysts*, 2009, **134**, 2385–2393.
36 G. Trusso Sfrazzetto, C. Satriano, G. A. Tomaselli and E. Rizzarelli, *Coord. Chem. Rev.*, 2016, **311**, 125–167.
37 S. K. Panigrahi and A. K. Mishra, *J. Photochem. Photobiol., C*, 2019, **41**, 100318.
38 L. Ai, Y. Yang, B. Wang, J. Chang, Z. Tang, B. Yang and S. Lu, *Sci. Bull.*, 2021, **66**, 839–856.
39 K. Yuan, X. Zhang, R. Qin, X. Ji, Y. Cheng, L. Li, X. Yang, Z. Lua and H. Liu, *J. Mater. Chem. C*, 2018, **6**, 12631–12637.
40 Si. Lu, L. Sui, J. Liu, S. Zhu, A. Chen, M. Jin and B. Yang, *Adv. Mater.*, 2017, **29**, 1603443.
41 P. Lesani, A. H. M. Haidi, Z. Lu, S. Palomba, E. J. New and H. Zreiqat, *Commun. Mater.*, 2021, **2**, 108.
42 X. Yang, L. Sui, B. Wang, Y. Zhang, Z. Tang, B. Yang and S. Lu, *Sci. Chin. Chem.*, 2021, **64**, 1547–1553.
43 Z.-H. Wena and X.-B. Yin, *RSC Adv.*, 2016, **6**, 27829–27835.
44 X. Li, S. Zhang, S. A. Kulinich, Y. Liu and H. Zeng, *Sci. Rep.*, 2014, **4**, 4976.
45 B. Demir, H. Moulahoum, F. Ghorbanizamani, F. B. Barlas, O. Yesiltepe, Z. P. Gumus, K. Meral, D. Odaci Demirkol and S. Timur, *J. Drug Deliv. Sci. Technol.*, 2021, **62**, 102363.
46 Q. Hu, X. Gong, L. Liu and M. M. F. Choi, *J. Nanomater.*, 2017, 30–37.
47 M. Akimowicz and J. Bucka-Kolendo, *Acta Biochim. Pol.*, 2020, **67**, 327–332.
48 P. Chandrasekaran, V. Arul and M. G. Sethuraman, *J. Fluoresc.*, 2020, **30**, 103–112.
49 G. Huang, X. Chen, C. Wang, H. Zheng, Z. Huang, D. Chen and H. Xie, *RSC Adv.*, 2017, **7**, 47840–47847.
50 G. Li Destri, L. Fichera, A. Zammataro, G. Trusso Sfrazzetto and N. Tuccitto, *Nanoscale*, 2019, **11**, 14203–14209.
51 A. Dager, T. Uchida, T. Maekawa and M. Tachibana, *Sci. Rep.*, 2019, **9**, 1–10.
52 F. Du, Y. Ming, F. Zeng, C. Yu and S. Wu, *Nanotechnology*, 2013, **24**, 365101.
53 S. Yang, X. Chen, S. Liu, F. Wang and G. Ouyang, *Talanta*, 2018, **186**, 80–87.
54 L. Li, L. Shi, Y. Zhang, G. Zhang, C. Zhang, C. Dong, H.-Z. Yu and S. Shuang, *Talanta*, 2019, **196**, 109–116.

55 M. Alafeef, K. Dighe and D. Pan, *ACS Appl. Mater. Interfaces*, 2019, **11**, 42943–42955.
56 F. Amato, M. C. P. Soares, T. Destri Cabral, E. Fujiwara, C. Monteiro de Barros Cordeiro, A. Criado, M. Prato and J. R. Bartoli, *ACS Appl. Nano Mater.*, 2021, **4**, 9738–9751.
57 M. Ganiga and J. Cyriac, *Sens. Actuators, B*, 2016, **225**, 522–528.
58 S. Menon, A. E. Vikraman, S. Jesny and K. G. Kumar, *J. Fluoresc.*, 2016, **26**, 129–134.
59 I. Costas-Mora, V. Romero, I. Lavilla and C. Bendicho, *Talanta*, 2015, **144**, 1308–1315.
60 M. Lan, Y. Di, X. Zhu, T.-W. Ng, J. Xi, W. Liu, X. Meng, P. Wang, C. S. Lee and W. Zhang, *Chem. Commun.*, 2015, **51**, 15574–15577.
61 Q. Mao, X. Kong, E. Shuang, J. Wang and X. Chen, *J. Mater. Sci.*, 2020, **55**, 16928–16939.
62 M. Zheng, Y. Li, Y. Zhang and Z. Xie, *RSC Adv.*, 2016, **6**, 83501–83504.
63 X. Sun, J. He, Y. Meng, L. Zhang, S. Zhang, X. Ma, S. Dey, J. Zhaoc and Y. Lei, *J. Mater. Chem. A*, 2016, **4**, 4161–4171.
64 B. B. Campos, R. Contreras-Càceres, T. J. Bandosz, J. Jimènez-Jimènez, E. Rodríguez-Castellòn, J. C. G. Esteves da Silva and M. Algarra, *Carbon*, 2016, **106**, 171–178.
65 G. E. LeCroy, K. A. S. Fernando, C. E. Bunker, P. Wang, N. Tomlinson and Y.-P. Sun, *Inorg. Chim. Acta*, 2017, **468**, 300–307.
66 D. Zhao, C. Chen, L. Lu, F. Yang and X. Yang, *Analyst*, 2015, **140**, 8157–8164.
67 M. Liang, Y. Chen, H. Zhang, X. Niu, L. Xu, C. Ren and X. Chen, *Analyst*, 2015, **140**, 6711–6719.
68 B. Sinduja and S. A. John, *Anal. Bioanal. Chem.*, 2019, **411**, 2597–2605.
69 C. Wang, Y. Ding, X. Bi, J. Luo, G. Wang and Y. Lin, *Sens. Actuators, B*, 2018, **264**, 404–409.
70 X. Lu, C. Liu, Z. Wang, J. Yang, M. Xu, J. Dong, P. Wang, J. Gu and F. Cao, *Nanomaterials*, 2018, **8**, 443.
71 S. Chen, C.-H. Xu, Y.-L. Yu and J.-H. Wang, *Sens. Actuators, B*, 2018, **266**, 553–560.
72 Xi. Qin, A. M. Asiri, K. A. Alamry, A. O. Al-Youbi and X. Sun, *Electrochim. Acta*, 2013, **95**, 260–267.
73 P. Shen and Y. Xia, *Anal. Chem.*, 2014, **86**, 5323–5329.
74 W. Liu, F. Ding, Y. Wang, L. Mao, R. Liang, P. Zou, X. Wang, Q. Zhao and H. Rao, *Sens. Actuators, B*, 2018, **265**, 310–317.
75 M. B, A. M. Raj and G. C. Thoma, *Sci. Rep.*, 2018, **8**, 13891.
76 F. Qu, W. Huang and J. You, *Colloids Surf., B*, 2018, **162**, 212–219.
77 G. Chellasamy, S. R. Ankireddy, K.-N. Lee, S. Govindaraju and K. Yun, *Mater. Today Bio*, 2021, **12**, 100168.
78 Y. Yang, D. Huo, H. Wu, X. Wang, J. Yang, M. Bian, Y. Ma and C. Hou, *Sens. Actuators, B*, 2018, **274**, 296–303.
79 Q. Wang, C. Wang, X. Wang, Y. Zhang, Y. Wu, C. Dong and S. Shuang, *Nanoscale*, 2019, **11**, 18845–18853.
80 S. V. Carneiro, V. H. R. de Queiroz, A. A. C. Cruz, L. M. U. D. Fechine, J. C. Denardin, R. M. Freire, R. F. do Nascimento and P. B. A. Fechine, *Sens. Actuators, B*, 2019, **301**, 127149.
81 D. P. Damera, R. Manimaran, V. V. K. Venuganti and A. Nag, *ACS Omega*, 2020, **5**, 19905–19918.
82 N. Tuccitto, L. Riela, A. Zammataro, L. Spitaleri, G. Li-Destri, G. Sfuncia, G. Nicotra, A. Pappalardo, G. Capizzi and G. Trusso Sfrazzetto, *ACS Appl. Nano Mater.*, 2020, **3**, 8182–8191.
83 R. Puglisi, A. Pappalardo, A. Gulino and G. Trusso Sfrazzetto, *ACS Omega*, 2019, **4**, 7550–7555.
84 Y. Fu, L. Huang, S. Zhao, X. Xing, M. Lan and X. Song, *Spectrochim. Acta Mol. Biomol. Spectrosc.*, 2021, **246**, 118947.
85 N. Tuccitto, L. Fichera, R. Ruffino, V. Cantaro, G. Sfuncia, G. Nicotra, G. Trusso Sfrazzetto, G. Li-Destri, A. Valenti, A. Licciardello and A. Torrisi, *ACS Appl. Nano Mater.*, 2021, **4**, 6250–6256.
86 S. W. Park, T. E. Kim and Y. K. Jung, *Anal. Chim. Acta*, 2021, **1165**, 338513.
87 Z. Shekarbeygi, C. Karami, E. Esmaeili, S. Moradi and M. Shahlaei, *Spectrochim. Acta Mol. Biomol. Spectrosc.*, 2021, **262**, 120148.
88 K. Li, M. Zhang, X. Ye, Y. Zhang, G. Li, R. Fuc and X. Chen, *RSC Adv.*, 2021, **11**, 29073–29079.
89 G.-Q. Zhang, X.-Y. Zhang, Y.-X. Luo, Y.-S. Li, Y. Zhao and X.-F. Gao, *Spectrochim. Acta, Part A*, 2021, **250**, 119384.
90 H. Li, J. Zhai, J. Tian, Y. Luo and X. Sun, *Biosens. Bioelectron.*, 2011, **26**, 4656–4660.
91 W. Lu, X. Qin, S. Liu, G. Chang, Y. Zhang, Y. Luo, A. M. Asiri, A. O. Al-Youbi and X. Sun, *Anal. Chem.*, 2012, **84**, 5351–5357.
92 X. Qin, W. Lu, A. M. Asiri, A. O. Al-Youbi and X. Sun, *Sens. Actuators, B*, 2013, **184**, 156–162.
93 W. Lu, X. Qin, A. M. Asiri, A. O. Al-Youbi and X. Sun, *J. Nanopart. Res.*, 2013, **15**, 1344.
94 M. Lan, J. Zhang, Y.-S. Chui, P. Wang, X. Chen, C.-S. Lee, H.-L. Kwong and W. Zhang, *ACS Appl. Mater. Interfaces*, 2014, **6**, 21270–21278.
95 V. Roshni and D. Ottoor, *J. Lumin.*, 2015, **161**, 117–122.
96 J. Liu, Y. Chen, W. Wang, J. Feng, S. Peng, S. Ma, H. Chen and X. Chen, *RSC Adv.*, 2016, **6**, 89916–89924.
97 R. Patidar, B. Rebary, G. R. Bhadu and P. Paul, *J. Lumin.*, 2016, **173**, 243–249.
98 J. Zhao, M. Huang, L. Zhang, M. Zou, D. Chen, Y. Huang and S. Zhao, *Anal. Chem.*, 2017, **89**, 8044–8049.
99 H. Abdolmohammad-Zadeh, Z. Azari and E. Pourbasheer, *Spectrochim. Acta, Part A*, 2021, **245**, 118924.
100 S. Liu, Y. Zhang, S. Gao, T. Fei and T. Zhang, *App. Surf. Sci.*, 2021, **544**, 148725.
101 H. Li, J. Zhai and X. Sun, *Langmuir*, 2011, **27**, 4305–4308.
102 M. Algarra, B. B. Campos, K. Radotic, D. Mutavdzic, T. Bandosz, J. Jimenez-Jimenez, E. Rodriguez-Castellon and J. C. G. Esteves da Silva, *J. Mater. Chem. A*, 2014, **2**, 8342–8351.
103 A. Cayuela, M. L. Soriano and M. Valcárcel, *Anal. Chim. Acta*, 2015, **872**, 70–76.
104 G. Liu, C. Xuan, D.-Q. Feng, D. Hua, T. Liu, G. Qi and W. Wang, *Anal. Methods*, 2017, **9**, 5611–5617.
105 Q. Wang and S. Zhang, *J. Lumin.*, 2014, **146**, 37–41.
106 P. Li, Y. Hong, H. Feng and S. F. Y. Li, *J. Mater. Chem. B*, 2017, **5**, 2979–2988.

107 L. Fang, L. Zhang, Z. Chen, C. Zhu, J. Liu and J. Zheng, *Mater. Lett.*, 2017, **191**, 1–4.
108 X. Liu, T. Li, Q. Wu, X. Yan, C. Wu, X. Chen and G. Zhang, *Talanta*, 2017, **165**, 216–222.
109 B. Fang, P. Wang, Y. Zhu, C. Wang, G. Zhang, X. Zheng, C. Ding, J. Gu and F. Cao, *RSC Adv.*, 2018, **8**, 7377–7382.
110 Y. Zhang, C. Li, L. Sun, J. Zhang, X. Yang and H. Ma, *Microchem. J.*, 2021, **169**, 106552.
111 M. L. Giuffrida, E. Rizzarelli, G. A. Tomaselli, C. Satriano and G. Trusso Sfrazzetto, *Chem. Commun.*, 2014, **50**, 9835–9838.
112 C. Satriano, G. Trusso Sfrazzetto, M. E. Amato, F. P. Ballistreri, A. Copani, M. L. Giuffrida, G. Grasso, A. Pappalardo, E. Rizzarelli, G. A. Tomaselli and R. M. Toscano, *Chem. Commun.*, 2013, **49**, 5565–5567.
113 S. Liu, J. Tian, L. Wang, Y. Zhang, X. Qin, Y. Luo, A. M. Asiri, A. O. Al-Youbi and X. Sun, *Adv. Mater.*, 2012, **24**, 2037–2041.
114 A. Zhu, Q. Qu, X. Shao, B. Kong and Y. Tian, *Angew. Chem., Int. Ed.*, 2012, **51**, 7185–7189.
115 P. Das, S. Ganguly, M. Bose, S. Mondal, A. K. Das, S. Banerjee and N. C. Das, *Mater. Sci. Eng. C*, 2017, **75**, 1456–1464.
116 A. Kumari, A. Kumar, S. Kumar Sahu and S. Kumar, *Sens. Actuators, B*, 2018, **254**, 197–205.
117 Y. Chen, Y. Lian, M. Huang, L. Wei and L. Xiao, *Analyst*, 2019, **144**, 4250–4257.
118 H. Liu, L. Jia, Y. Wang, M. Wang, Z. Gao and X. Ren, *Anal. Bioanal. Chem.*, 2019, **411**, 2531–2543.
119 M. Lan, S. Zhao, S. Wu, X. Wei, Y. Fu, J. Wu, P. Wang and W. Zhang, *Nano Res.*, 2019, **12**, 2576–2583.
120 J. Y. Tai, K. H. Leong, P. Saravanan, S. T. Tan, W. C. Chong and L. C. Sim, *J. Environ. Chem. Eng.*, 2021, **9**, 104622.
121 K. Qu, J. Wang, J. Ren and X. Qu, *Chem.–Eur. J.*, 2013, **19**, 7243–7249.
122 J. F. Y. Fong, S. F. Chin and S. M. Ng, *Sens. Actuators, B*, 2015, **209**, 997–1004.
123 H. Hamishehkar, B. Ghasemzadeh, A. Naseri, R. Salehi and F. Rasoulzadeh, *Spectrochim. Acta, Part A*, 2015, **150**, 934–939.
124 M. Zhou, Z. Zhou, A. Gong, Y. Zhang and Q. Li, *Talanta*, 2015, **143**, 107–113.
125 J. Feng, Y. Chen, Y. Han, J. Liu, C. Ren and X. Chen, *Anal. Chim. Acta*, 2016, **926**, 107–117.
126 G. Li, N. Lv, W. Bi, J. Zhang and J. Ni, *New J. Chem.*, 2016, **40**, 10213–10218.
127 M. Zulfajri, G. Gedda, C.-J. Chang, Y.-P. Chang and G. G. Huang, *ACS Omega*, 2019, **4**, 15382–15392.
128 W. Li, Y. Liu, B. Wang, H. Song, Z. Liu, S. Lu and B. Yang, *Chin. Chem. Lett.*, 2019, **30**, 2323–2327.
129 Q. Hu, Y. Pan, X. Gong, S. Rao, L. Xiao, L. Liu and Z. Yang, *Food Chem.*, 2020, **308**, 125590.
130 Z. Nan, C. Hao, X. Zhang, H. Liu and R. Sun, *Spectrochim. Acta, Part A*, 2020, **228**, 117717.
131 S. S. Wee, Y. H. Ng and S. M. Ng, *Talanta*, 2013, **116**, 71–76.
132 Y. Gao, Y. Jiao, H. Zhang, W. Lu, Y. Liu, H. Han, X. Gong, L. Li, S. Shuang and C. Dong, *J. Mater. Chem. B*, 2019, **7**, 5502–5509.
133 S. Chen, M.-X. Liu, Y.-L. Yu and J.-H. Wang, *Sens. Actuators, B*, 2019, **288**, 749–756.
134 Y. Hu, W. Ji, J. Sun, X. Liu, R. Zhou, J. Yan and N. Zhang, *Luminescence*, 2021, **36**, 1385–1394.
135 A. Ghosh and G. Das, *New J. Chem.*, 2021, **45**, 8747–8754.
136 K. M. Tripathi, T. S. Tran, Y. J. Kim and T. Y. Kim, *ACS Sustainable Chem. Eng.*, 2017, **5**, 3982–3992.
137 A. Cayuela, M. L. Soriano, M. C. Carrión and M. Valcárcel, *Anal. Chim. Acta*, 2014, **820**, 133–138.
138 S. Mohapatra, S. Sahu, S. Nayak and S. K. Ghosh, *Langmuir*, 2015, **31**, 8111–8120.
139 Y. Ding, J. Ling, J. Cai, S. Wang, X. Li, M. Yang, L. Zha and J. Yan, *Anal. Methods*, 2016, **8**, 1157–1161.